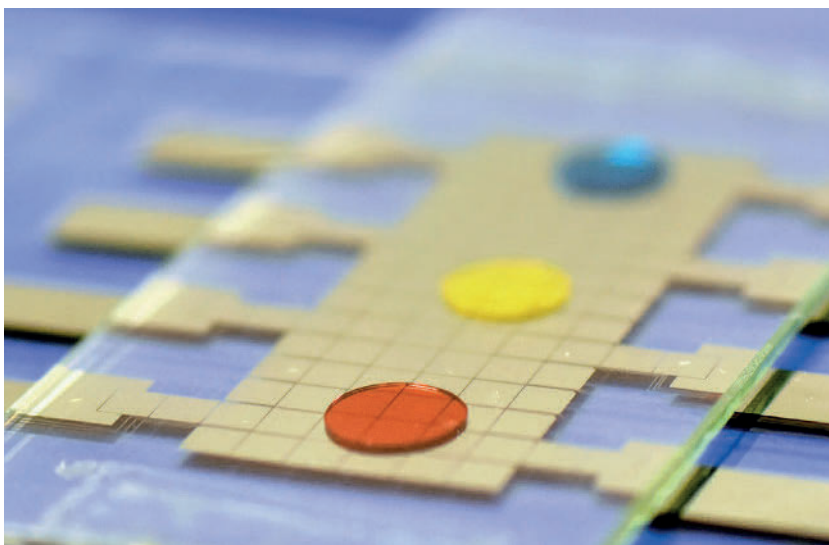


DOCTORAL SCHOOL IN NATURAL SCIENCES DISSERTATION SERIES  
UNIVERSITY OF HELSINKI

**GOWTHAM SATHYANARAYANAN**

## **DIGITAL MICROFLUIDICS FOR DRUG METABOLISM RESEARCH IN DROPLET-SCALE**



DRUG RESEARCH PROGRAM  
DIVISION OF PHARMACEUTICAL CHEMISTRY AND TECHNOLOGY  
FACULTY OF PHARMACY  
DOCTORAL PROGRAMME IN MATERIALS AND NANOSCIENCES  
UNIVERSITY OF HELSINKI

Drug Research Program  
Division of Pharmaceutical Chemistry and Technology  
Faculty of Pharmacy  
University of Helsinki

# **DIGITAL MICROFLUIDICS FOR DRUG METABOLISM RESEARCH IN DROPLET-SCALE**

**Gowtham Sathyanarayanan**

DOCTORAL DISSERTATION

To be presented for public discussion, with the permission of the Faculty of  
Pharmacy of the University of Helsinki, in lecture hall 2041, Biocenter 2,  
on the 18<sup>th</sup> of September, 2020, at 12 o'clock.

Helsinki 2020

<b>Supervisor</b>	Docent Tiina Sikanen Drug Research Program Division of Pharmaceutical Chemistry and Technology Faculty of Pharmacy University of Helsinki Helsinki, Finland
<b>Co-supervisor</b>	Dr Markus Haapala Drug Research Program Division of Pharmaceutical Chemistry and Technology Faculty of Pharmacy University of Helsinki Helsinki, Finland
<b>Reviewers</b>	Assistant Professor Steve Shih Department of Electrical and Computer Engineering Concordia University Montreal, Canada  Adjunct Professor Séverine Le Gac Faculty of Electrical Engineering, Mathematics and Computer Science University of Twente Enschede, The Netherlands
<b>Opponent</b>	Professor Pasi Kallio Faculty of Medicine and Health Technology Tampere University Tampere, Finland

© Gowtham Sathyanarayanan

ISBN 978-951-51-6453-7 (paperback)

ISBN 978-951-51-6454-4 (PDF)

ISSN 2669-882X (print)

ISSN 2670-2010 (online)

<http://ethesis.helsinki.fi>

The Faculty of Pharmacy uses the Urkund system (plagiarism recognition) to examine all doctoral dissertations

Published in

*Doctoral School in Natural Sciences Dissertation Series University of Helsinki*

Painosalama Oy, Turku, Finland 2020

## Abstract

Drug metabolism is a detoxification process by which the body converts pharmaceuticals into more hydrophilic metabolites. Understanding of the drug metabolism process and metabolic profiling plays a vital role in drug development processes by ensuring the safety and efficacy of treatments. Cytochromes P450 (CYP) are a superfamily of enzymes that are primarily responsible for metabolizing the majority of clinically relevant drugs. In preclinical drug development research, there is a constant need for the identification of metabolites and their CYP isoenzyme-specific elimination route, as well as possible drug-drug interactions thereof using high speed *in vitro* techniques. Miniaturization of the drug metabolism assays and related processes could further improve the throughput via parallelism and integration of several analytical steps on a single platform, as well as reducing the consumption of expensive reagents substantially.

Micro total analysis systems ( $\mu$ TAS) usually refer to microfabricated devices that integrate several analytical unit operations, such as sample preparation, extraction, separation, and analysis on a single platform. These  $\mu$ TAS platforms can be either continuous-flow microchannel based systems or discrete droplet systems. Digital microfluidics (DMF) is one such technology, where sample droplets are manipulated individually on an array of electrodes. In DMF, the droplets of hundreds of nanolitres to a few microliters of volume can be dispensed, split, mixed, and merged independently via programmed and automated voltage application. In this thesis, several DMF-based bioanalytical concepts were developed and their feasibility for implementing droplet-scale drug metabolism assays was evaluated.

In the first sub-project, droplet-scale immobilized enzyme reactors were developed by immobilizing CYP enzymes on porous polymer monoliths affixed onto a DMF platform. Assay incubation at physiological temperature was facilitated by localized heating of the DMF platform using integrated inkjet-printed microheaters. For the on-chip detection of drug metabolites, a protocol facilitating interfacing of the DMF device with a commercial wellplate reader was developed.

In the second sub-project, the developed DMF platform, featuring the CYP reactors, were interfaced with ambient mass spectrometry (MS) via desorption atmospheric pressure photoionization (DAPPI). For *in situ* identification of the drug metabolites by DAPPI-MS, the chip design was optimized to be able to control the critical surface sensitive processes, such as sample precipitation and subsequent desorption/ionization directly from DMF surfaces. In addition, the feasibility of the same platform for a droplet-based liquid-liquid extraction of pharmaceuticals was demonstrated. All pharmaceuticals and metabolites analyzed could be detected with lower limits of detection in the range of a few picomoles.

In the third sub-project, DMF droplet manipulation was interfaced with channel microfluidics to facilitate more versatile sample preparation such as separation of target analytes after the droplet-based enzyme reactions and prior to detection. To support the scaling up of the developed technology toward mass manufacturing, the entire device was assembled using low-cost inkjet printing and cleanroom-free polymer processing techniques. To achieve this interfacing, off-stoichiometric thiol-ene (OSTE) polymers were

introduced as a new alternative dielectric material for the coating of inkjet-printed DMF electrode arrays, as well as for the integration of the microchannels with a DMF platform.

In the fourth sub-project, magnetic bead based enzyme immobilization protocol was developed to facilitate screening the individual variation of CYP activities in donor-derived human liver microsomes (HLM) in droplet-scale. A CYP1A isoenzyme-specific model reaction was chosen to assess the inter-individual variation in the activities of this metabolic route in the liver microsomes collected from five individuals. The demonstrated protocol was shown to be technically feasible for biopsy-scale samples.

In all, the new droplet-scale concepts developed in this thesis are first-in-their-kind examples of droplet-scale drug metabolism assays on DMF platform. The methods developed are generally qualitative or semi-quantitative and thus, in their present form, best feasible for the preliminary determination of metabolic clearance via CYP or identification of the produced metabolites of new drug candidates *in vitro*. Further development of the technology, particularly the enzyme immobilization process and the quantification of the produced metabolites, is needed to improve the wider applicability of the assays. It is noteworthy however that all of the fabrication processes and interfacing approaches taken in this thesis were carried out in regular, cleanroom-free laboratory conditions, which is foreseen to significantly improve the adaptability of the technology in any bioanalytical laboratories.

## Preface

This work has been carried out at the Division of Pharmaceutical Chemistry and Technology, Faculty of Pharmacy, University of Helsinki (UH), Finland during the years 2015–2020. Parts of the work (Publication III) has been carried out in collaboration with Wheeler Microfluidics Laboratory, University of Toronto, Canada. Centre for International Mobility, UH Research Foundation, and the European Research Council are acknowledged for funding this work. I also acknowledge Doctoral School of Natural Sciences, UH for dissertation completion grant and Doctoral Programme in Materials Research and Nanosciences, UH for the travel grants for conference and research visits.

First of all, I express my sincere gratitude to my supervisors Dr. Tiina Sikanen and Dr. Markus Haapala. I am forever grateful to Tiina for the opportunity to work in the Chemical Microsystems (CheMiSys) research group and for her guidance and support during these years. I thank her for both the positive and critical comments during these years which made it possible for me to finish my PhD work. I admire and appreciate her “*Sisu*.” Also, because of this opportunity I get to spend and experience 5+ years of my life in Finland, “*kaunis maa*” which I will cherish forever. I acknowledge Markus, my co-supervisor, colleague and friend for his contributions in the lab, valuable comments and numerous fruitful discussions. I also thank him for introducing the best foods in the city, barbecues, ice-creams and being a window to the Finnish culture to me.

Special thanks to the supervisors, preliminary examiners, custos, opponent and Viikki-PhD services for their contributions and timely responses despite the COVID-19 pandemic situation. I acknowledge the co-authors and collaborators: Iiro Kiiski for the enzyme immobilization protocol, and Dr. Christopher Dixon and Prof. Aaron Wheeler for the collaborative work on the inkjet-printing of microdevices. I am also thankful to Chris and Prof. Wheeler for hosting me during my research visit to University of Toronto in 2017. Special thanks to Dr. Ryan Fobel (Sci-Bots, Canada) for his technical support for the DropBot open-source automation system. I thank Dr. Ville Jokinen (Aalto University, Finland) and Prof. Tapio Kotiaho (UH) for being my thesis steering group members. Dr. Steve Shih (Concordia University, Canada) and Dr. Séverine Le Gac (University of Twente, The Netherlands) are acknowledged for acting as the preliminary examiners and reviewing this thesis. Prof. Jari Yli-Kauhaluoma (UH) and Prof. Pasi Kallio (Tampere University, Finland) are thanked for acting as the custos and the opponent, respectively.

I thank all the former and present colleagues of Division of Pharmaceutical Chemistry and Technology (UH). I really enjoyed our division’s innovative and fun-filled “*pikkujoulu*” Christmas parties and also enjoyed being part of our crazy BBQ events. Warm thanks to all the members of my “CheMiSys” family. Sari and Elisa always helped me with several practical issues without any hesitation. Ashkan always brought joy, positivity and sometime delicious cakes to work. I enjoyed travelling to conferences, and sharing thoughts and depressing realities with Iiro and Kati. I also thank Ciler, Tea, Vera, Päivi, and Sanja for creating a warm and healthy working atmosphere. I had fun during our “each and every” lab outings and activities, dinners and Pompiers lunches amidst crazy and stressful times at work.

I am thankful to my previous mentors: Prof. D. Balasubramanian (LVPEI, India) for inspiring me to choose the scientific career; Prof. M. Sridharan (SASTRA University, India) for introducing me to the field of microfluidics and providing me an opportunity to pursue my master thesis abroad; and Prof. David Amabilino and Dr. Romén Rodríguez-Trujillo for training me in microfluidics, materials characterization and scientific writing during my thesis work in University of Barcelona, Spain.

Life would have been tougher during these years without my Helsinki friends. They have made these years fun and colourful through countless meets, outings, unicafe/kartano conversations, delicious dinners, travelling, cycling, etc. Special thanks to my Indo-Finnish music band members for the crazy jamming sessions and providing me an opportunity to perform in various events. Because of “Finland Tamil Sangam (FINTA),” I did not miss my home much during important Indian and Tamil festivals. I thank them for organizing such events and serving “*Ilai saapadu*” in Finland. I am particularly thankful to Maitry, Rishi, Gungan, Sitaram, Neha, Jai, Palash, and Thomas who became my close friends during these years. They are my second family away from home and I wish to have their friendship forever. This list is incomplete without thanking Reena and words cannot describe how grateful I am to her. She has been encouraging and supportive throughout the entirety of my research career, from LVPEI days in 2013 till now. Her motivation, endless support and presence made it possible for me to complete my PhD work. Thank you for standing beside me.

I am thankful to my “*thalaiyur-kollumangudi*” family for their constant support and encouragement. I try to meet their high hopes on me even though I will not be a “Medical Doctor” as some of them wanted. Finally, I am deeply indebted to Sudha Sathyanarayanan, my mother; Sathyanarayanan Sethuraman, my father; and Thvija Sathyanarayanan, my sister. They always had faith in me and encouraged me to pursue the education and career path I wanted. Without their support and love, it would not have been possible for me to persevere and achieve my goals.

Helsinki, August 2020

*Gowtham Sathyanarayanan*

**தினையளவு போதாச் சிறுபுல் நீர்கண்ட  
பனையளவு காட்டும் படித்தால்**

(A droplet as tiny as a millet can project information as big as a palm tree, if examined)

-கபிலர் (Kapilar, 1<sup>st</sup> century CE)



# Contents

Abstract	3
Preface	5
Contents	8
List of original publications	10
Abbreviations	13
1 Introduction	15
1.1 Digital microfluidics (DMF)	17
1.1.1 Fundamentals	17
1.1.2 Fabrication and implementation	18
1.1.3 Detection	20
1.1.4 Advantages and current challenges of DMF in chemical biology	21
1.2 Significance of metabolism to safety and efficacy of drugs	23
1.2.1 Role in pre-clinical drug development <i>in vitro</i>	23
1.2.2 Role in drug dosing	24
1.2.3 Miniaturization of drug metabolism assays	25
2 Aims of the study	27
3 Materials, instrumentation and standard methods	28
3.1 Chemicals, microfabrication materials and instrumentation	28
3.2 Standard methods and protocols	31
4 Experimental methods developed in the thesis	33
4.1 Microchip designs, fabrication and operation	33
4.2 Microheater fabrication and characterization	36
4.3 Enzyme immobilization	38
4.4 Drug metabolism and drug distribution assays	39
4.5 Analytical method interfaces	42

5 Results and discussion	46
5.1 Selection of dielectric material	46
5.2 Digital-to-channel microfluidic interface	49
5.3 Development of droplet-scale CYP reactors	51
5.3.1 Heating of CYP reactors and evaporation effects	51
5.3.2 Selection of enzyme immobilization approaches	52
5.3.3 Mass spectrometry detection of metabolites	54
5.4 Digital microfluidics for determining personalized drug clearance	56
6 Summary and conclusions	58
References	60

## List of original publications

This thesis is based on the following publications:

- I            “Digital microfluidic immobilized cytochrome P450 reactors with integrated inkjet-printed microheaters for droplet-based drug metabolism research”:  
**Gowtham Sathyanarayanan**, Markus Haapala, Iiro Kiiski, and Tiina Sikanen, *Analytical and Bioanalytical Chemistry*, 410 (25), 6677–87, 2018. DOI: 10.1007/s00216-018-1280-7
  
- II           “Integrating digital microfluidics with ambient mass spectrometry using SU-8 as dielectric layer”:  
**Gowtham Sathyanarayanan**, Markus Haapala, and Tiina Sikanen *Micromachines*, 9 (12), 649, 2018. DOI: 10.3390/mi9120649
  
- III          “A digital-to-channel microfluidic interface via inkjet printing of silver and UV curing of thiol-enes”:  
**Gowtham Sathyanarayanan**,\* Markus Haapala,\* Christopher Dixon,\* Aaron Wheeler, and Tiina Sikanen: *Advanced Materials Technologies*, 2020, 2000451. DOI: 10.1002/admt.202000451
  
- IV          “Digital microfluidics-enabled analysis of individual variation in liver cytochrome P450 activity”:  
**Gowtham Sathyanarayanan**, Markus Haapala, and Tiina Sikanen, 2020 (Unpublished manuscript).

\* These authors contributed equally to the work (III).

The publications are referred to in the text by their roman numerals.

### **Author's contribution to the publications included in the thesis:**

- I            Author designed the microchips, microheaters, and the experiments together with Markus Haapala and Tiina Sikanen. Author carried out microchip- and microheater fabrication, related method development and enzymatic assays. Iiro Kiiski developed the enzyme immobilization protocol. Markus Haapala conducted IR- and SEM imaging with the help of author. Author wrote the manuscript with contributions from co-authors.
  
- II           Author designed the microchips and experiments together with Markus Haapala and Tiina Sikanen. Author carried out microchip fabrication, related method development, and enzymatic assays. Author conducted mass spectrometry measurements and related data analysis together with Markus Haapala. Author wrote the manuscript with contributions from co-authors.
  
- III          Author designed the microchips and experiments together with Christopher Dixon and Markus Haapala, and with the help of Tiina Sikanen. Author, Christopher Dixon and Markus Haapala contributed equally to the experimental work with the following primary responsibility areas: microchip fabrication (Haapala), characterization of the dielectric performance (Dixon), and electrophoresis experiments (author). Author and Christopher Dixon wrote the manuscript with contributions from co-authors.
  
- IV          Author designed the microchips and experiments together with Markus Haapala and Tiina Sikanen. Author carried out microchip fabrication, related method development, and enzymatic assays. Author wrote the manuscript with contributions from co-authors.

Publication III was also included in the dissertation of Dr. Christopher Dixon from the University of Toronto, Canada.

**The work presented in this thesis has also been presented in the following international peer-reviewed conference proceedings:**

1. Iiro Kiiski, Sari Tähkä, **Gowtham Sathyanarayanan**, Markus Haapala, Ville Jokinen, and Tiina Sikanen. “Immobilized cytochrome P450 microreactors with integrated heaters.” *Proceedings of the 20<sup>th</sup> International Conference on Miniaturized Systems for Chemistry and Life Sciences (MicroTAS2016)*, Dublin, Ireland, 2016, pp. 645–646.
2. **Gowtham Sathyanarayanan**, Markus Haapala, and Tiina Sikanen: “Drug metabolism in droplet scale with on-chip metabolite identification by ambient mass spectrometry.” *Proceedings of the 22<sup>nd</sup> International Conference on Miniaturized Systems for Chemistry and Life Sciences (MicroTAS2018)*, Kaohsiung, Taiwan, 2018, pp.1973–1975.
3. **Gowtham Sathyanarayanan**, Markus Haapala, and Tiina Sikanen: “Drug metabolism-in-a-droplet: A digital microfluidic approach toward precision medicine.” *Proceedings of the 23<sup>rd</sup> International Conference on Miniaturized Systems for Chemistry and Life Sciences (MicroTAS2019)*, Basel, Switzerland, 2019, pp. 868–869.

**Parts of the work presented in this thesis has also been presented at the following international conferences:**

1. **Gowtham Sathyanarayanan**, Markus Haapala, and Tiina Sikanen: “Integrating digital microfluidic sample preparation with desorption atmospheric pressure photoionization-mass spectrometry.” *21<sup>st</sup> International Mass Spectrometry Conference (IMSC2016)*, Toronto, Canada, 2016.
2. **Gowtham Sathyanarayanan**, Markus Haapala, and Tiina Sikanen: “Digital microfluidic enzyme reactor with integrated low-cost printed microheater.” *International Conference on Micro and Nano Engineering (MNE2017)*, Braga, Portugal, 2017.
3. **Gowtham Sathyanarayanan**, Markus Haapala, and Tiina Sikanen: “Digital microfluidic enzyme reactor with integrated low-cost printed microheater.” *MicroNano Systems Workshop (MSW)*, Espoo, Finland, 2018.

**Parts of the work presented in this thesis has also been published as the following application note:**

1. **Gowtham Sathyanarayanan**, Päivi Järvinen, and Tiina Sikanen: “Quantification of digital microfluidic fluorescence assays with the Varioskan LUX Multimode Microplate Reader.” Application note, *ThermoFisher Scientific*, 2018. DOI: 10.13140/RG.2.2.23726.15686

## Abbreviations

ACN	acetonitrile
AD	analog-to-digital
ADME	absorption, distribution, metabolism, and excretion
a.u.	arbitrary unit
b-FL	biotinylated fusogenic liposomes
b-HLM	biotinylated human liver microsomes
ca.	approximately
CAD	computer-aided design
CEC	3-cyano-7-ethoxycoumarin
CHC	3-cyanoumbelliferone
CVD	chemical vapour deposition
CYP	cytochrome P450 (enzyme superfamily)
DAPPI	desorption atmospheric pressure photoionization
DBF	dibenzylfluorescein
DMF	digital microfluidics
EIC	extracted ion chromatogram
ER	endoplasmic reticulum
EROD	ethoxyresorufin-O-deethylation
ESI	electrospray ionization
EWOD	electrowetting-on-dielectric
ex/em	excitation/emission wavelengths
FDA	the United States Food and Drug Administration
HLM	human liver microsome
HV	high voltage
IC50	half maximal inhibitory concentration
IMER	immobilized enzyme (micro) reactor
IR	infrared
ITO	indium tin oxide
LLE	liquid-liquid extraction
(L)LOD	(lower) limit of detection
logD	octanol-water distribution coefficient
LOQ	limit of quantification
M <sup>+</sup>	radical cation of species M
[M+H] <sup>+</sup>	protonated ion of species M
MALDI	matrix assisted laser desorption ionization
MCE	microchip capillary electrophoresis
MS	mass spectrometry
<i>m/v</i>	mass/volume
<i>m/z</i>	mass-to-charge ratio
N/A	not applicable
NADPH	β-nicotinamide adenine dinucleotide 2'-phosphate
NIMS	nanostructure-initiator mass spectrometry

NMR	nuclear magnetic resonance
OSTE	off-stoichiometry thiol-ene
PBS	phosphate-buffered saline
PCB	printed circuit board
PCR	polymerase chain reaction
PDMS	poly(dimethylsiloxane)
PET	poly(ethylene terephthalate)
$pK_a$	negative base-10 logarithm of acid dissociation constant ( $K_a$ )
PMMA	poly(methylmethacrylate)
PMT	photomultiplier tube
rpm	revolution per minute
(R)SD	(relative) standard deviation
RT	room temperature
SEM	scanning electron microscope
TFA	trifluoroacetic acid
UV	ultraviolet
$V_{rms}$	root mean square voltage
$v/v$	volume/volume
w.r.t.	with respect to
$\Delta T$	temperature difference
$\mu$ TAS	micro total analysis system

# 1 Introduction

Drug metabolism is the process by which clinically relevant drugs and other xenobiotics are transformed into more hydrophilic metabolites by the human body through enzymatic reactions taking place primarily in the liver.<sup>[1]</sup> Understanding the drug-drug interactions inside the body is crucial in assessing the safety and efficacy of the drug. Analyzing drug elimination (metabolism) from the body is vital in determining the speed and the route of drug elimination. Drug efficacy, such as binding to the target receptors, can be predicted with the help of computational tools.<sup>[2]</sup> However, drug metabolism, particularly enzyme kinetics, is challenging to predict by computation tools and thus, often requires extensive *in vitro* and *in vivo* experimentation before the safety and efficacy of the new drug candidate can be assured.<sup>[3]</sup> Additionally, drug metabolism also plays a significant role in the post-marketing evaluation of the drug safety of critically ill patients by precisely calculating the dosage.<sup>[4]</sup>

After administration, the disposition of the drug undergoes the following steps inside the body: absorption, distribution, metabolism, and elimination, which can simply be referred to as ADME. Among these, metabolism is the process by which the drug molecules are converted into more water-soluble form primarily by the liver enzymes. In the body, drug metabolism is carried out in two phases: (i) modification of the drug molecule into a more reactive polar molecule via redox reactions (e.g., dealkylation and hydrolysis) in Phase I metabolism, and (ii) further modification of the molecule with additional species, such as glucuronic acid, glutathione, etc. via conjugation in Phase II metabolism. Cytochromes P450 (CYP) is the superfamily of enzymes that are responsible for the Phase I biotransformation of around 70–80% of all pharmaceutical drugs.<sup>[5]</sup> Thus, understanding the disposition of a new drug candidate by the specific CYP enzyme is a crucial step in pre-clinical drug development.<sup>[6]</sup> This screening of the isoenzyme specific metabolism of drugs is a time-consuming and resource demanding process (Figure 1). From 5,000 to 10,000 possible candidates, only one new drug gets approved to enter the market and the entire drug development process typically takes up to 11–16 years.<sup>[7]</sup> Therefore, increasing the efficiency of the metabolic screening would benefit the pre-clinical drug discovery and development process.



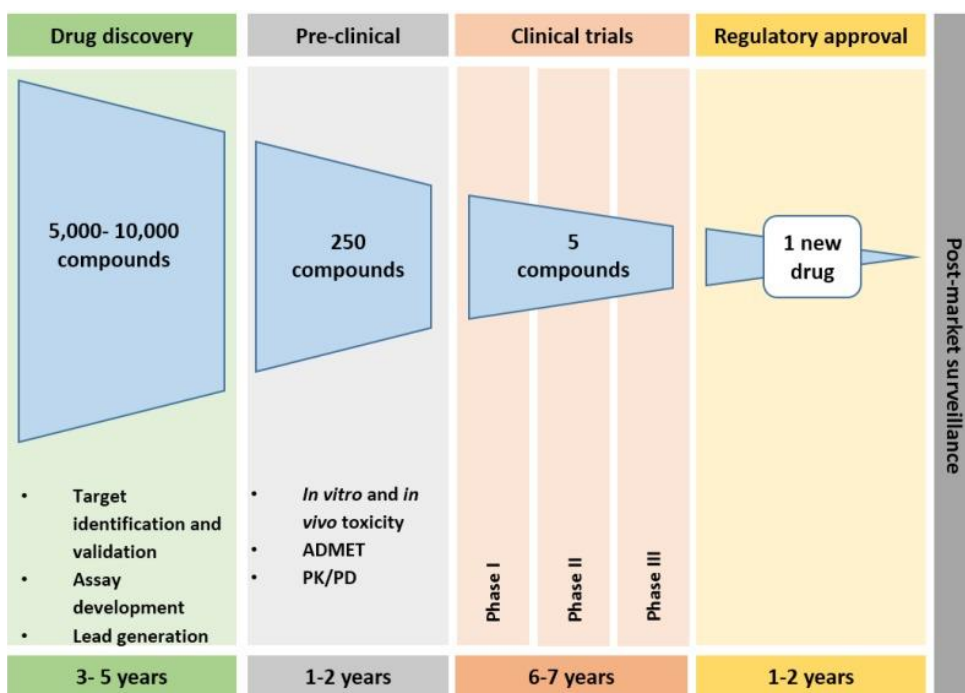


**Figure 1** Drug discovery and development timeline (ADMET-Absorption, Distribution, Metabolism, Excretion, Toxicology; PK-pharmacokinetics; PD-pharmacodynamics). Reprinted from ref. [7] © 2016 by Matthews et al.; MDPI, CC BY 4.0.

The miniaturization of analytical systems has been well established in chemical and biological research in recent decades to improve the speed of analysis and decrease the cost. Via miniaturization, multiple units of chemical analysis, such as sample preparation, separation, and detection, can be combined into a single device—a micro total analysis system ( $\mu$ TAS).<sup>[8]</sup>  $\mu$ TAS improves analysis by reducing the sample volume and thus, the waste, and by increasing the speed of analysis. Microfluidic ( $\mu$ TAS) systems are extensively used in a variety of biological applications, such as enzymatic, immunological, diagnostic, and cell-based assays, where the reactions and analyses are carried out in a single platform.<sup>[9]</sup> These microfluidic systems are often called lab-on-a-chip devices nowadays, as the entire functional units of laboratory processes can be miniaturized on a single microfluidic chip.<sup>[10]</sup> Using lab-on-a-chip technologies in pre-clinical drug development has gained interest in recent years because of their rapidity, cost-effectiveness, and the possibility of substantially reducing the consumption of expensive reagents and drugs.<sup>[11]</sup>

Digital microfluidics (DMF) is a droplet-based microfluidic technology, where individual sample droplets (reactors) are handled via electrowetting-on-a-dielectric (EWOD) in an automated fashion and it has been widely used in immunological and diagnostic assays over the past decade.<sup>[12]</sup> The term DMF may sometimes refers to other droplet actuation systems, including water-in-oil or oil-in-water emulsion based droplet microfluidics. Apart from the EWOD-driven DMF, there are also other approaches to manipulate droplets on surfaces via magnetic force,<sup>[13]</sup> surface acoustic waves,<sup>[14]</sup> and thermocapillary force.<sup>[15]</sup> However, in the context of this thesis, DMF solely refers to (non-optical) EWOD-based microdevices. Unlike other microfluidic systems, DMF does not suffer from complex sample loading via tubings and pumps. As a result, there are practically

no dead volumes in DMF systems. This is particularly important in the case of expensive reagents, drugs and biological samples. Furthermore, DMF allows the usage of complex sample matrices, including solid particles and live cells, without any clogging or precipitation as in the channels. Owing to its compact size, the system is also portable and can be used in point-of-care diagnostic trials.<sup>[16]</sup> In addition, DMF has been interfaced with many analytical methods, such as optical, electrochemical, mass spectrometry, and NMR, which allows the user to analyze almost any type of biologically relevant analytes.<sup>[17]</sup>

This thesis explores the feasibility of DMF technology to realize drug metabolism research in droplet-scale. In the following sections, the theoretical frame and state-of-the-art DMF technology (Section 1.1), as well as the real-world implications of drug metabolism (Section 1.2), will be reviewed.

## 1.1 Digital microfluidics (DMF)

### 1.1.1 Fundamentals

Microfluidics refers to the science and manipulation of fluids of picoliter to microliter volume inside channels with the dimensions of tens to hundreds of micrometers.<sup>[18]</sup> A microfluidic device in its most common format consists of microchannel(s), where the liquids are pumped with the help of spontaneous capillary forces, pressure gradients, or electric fields (Figure 2a). However, this study focuses on discrete droplet systems called digital microfluidics.<sup>[12]</sup> Digital microfluidics (DMF) is a droplet-handling technology, where discrete droplets of liquid are manipulated on a surface by using an electric field in an air or oil filled medium. This is not to be confused with droplet microfluidics, which by default, refers to sample droplets manipulated inside a microchannel filled with a continuous phase, another immiscible liquid (Figure 2b).<sup>[19]</sup> In DMF, the sample droplets are moved or actuated by selectively wetting the inherently hydrophobic dielectric surface by applying voltage, a phenomenon called EWOD.<sup>[20–22]</sup> By exploiting EWOD, one can perform fluidic operations, such as the splitting, dispensing, mixing, rinsing, and merging of droplets by applying the voltages selectively (Figure 2c).<sup>[23]</sup> Like the channel-based microfluidics, DMF can also be integrated with many analytical techniques, which makes it a potential miniaturized technology for various bioanalytical applications.<sup>[17]</sup> However, DMF has certain benefits that are not present in channel-based microfluidics: (i) no need of auxiliary fluidic components, such as pumps, valves, tubing, or external mixers since all of the fluidic operations are controlled via electrowetting; (ii) multiple droplets (reactions) can be manipulated in parallel on a single device with a compact design; (iii) droplet operations are programmable and re-configurable via automation since the devices can use a generic array of electrodes; and (iv) samples containing solid particles, beads, and cells can be manipulated on DMF without the risk of clogging.

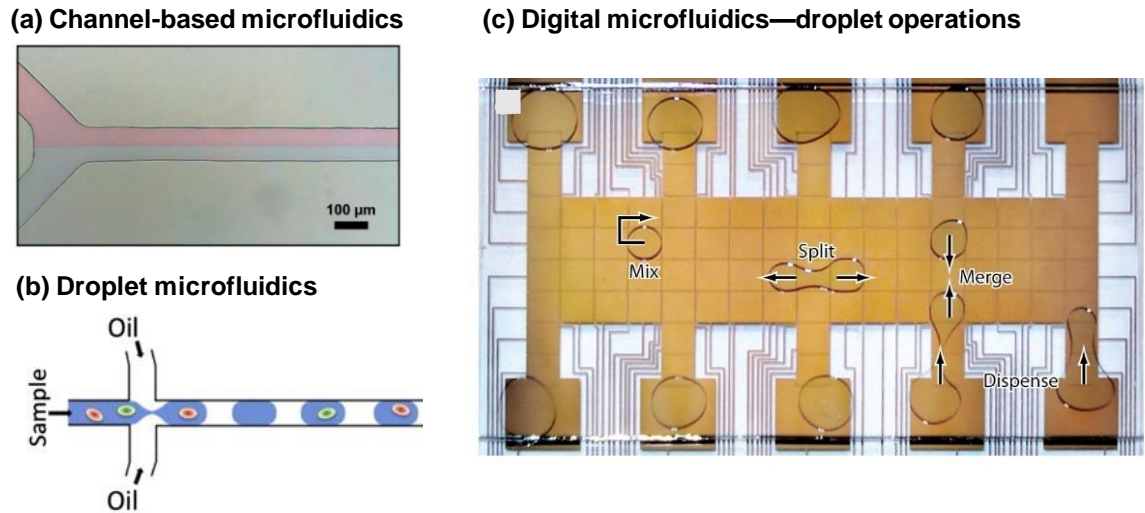


**Figure 2** (a) Photograph of a simple y-shaped microfluidic channel. Modified and reprinted from ref. [24], © 2013 by Orabona et al.; MDPI, CC BY 3.0. (b) Schematic illustration of droplet microfluidics. Modified and reprinted with permission from ref. [25], © 2014 by Elsevier. (c) Droplet operations in digital microfluidics (DMF). Modified and reprinted with permission from ref. [12], © 2012 by Annual Reviews.

In general, DMF devices are categorized between two configurations: one-plate open-to-air systems<sup>[20]</sup> and two-plate closed systems.<sup>[22]</sup> In one-plate devices, the positive actuation and ground electrodes are fabricated in parallel (Figure 3a). In two-plate devices, the actuation electrodes are at the bottom and a continuous conductive top plate acts as a ground electrode (Figure 3b). Two-plate DMF devices are more common in biological applications because of their advantages over one-plate configurations in terms of the dispensing of droplets from a larger reservoir of electrodes and lower rate of sample evaporation during prolonged incubations.

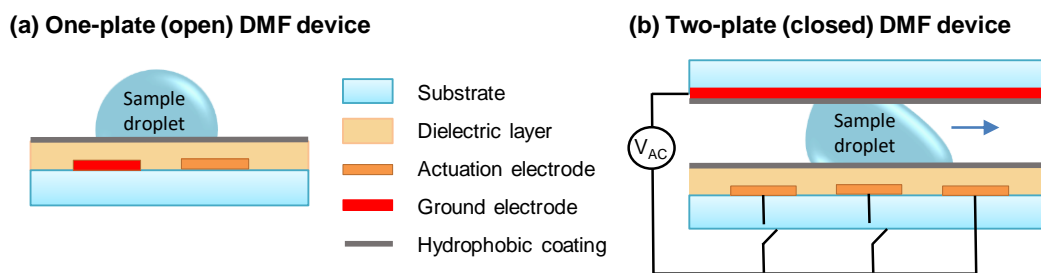


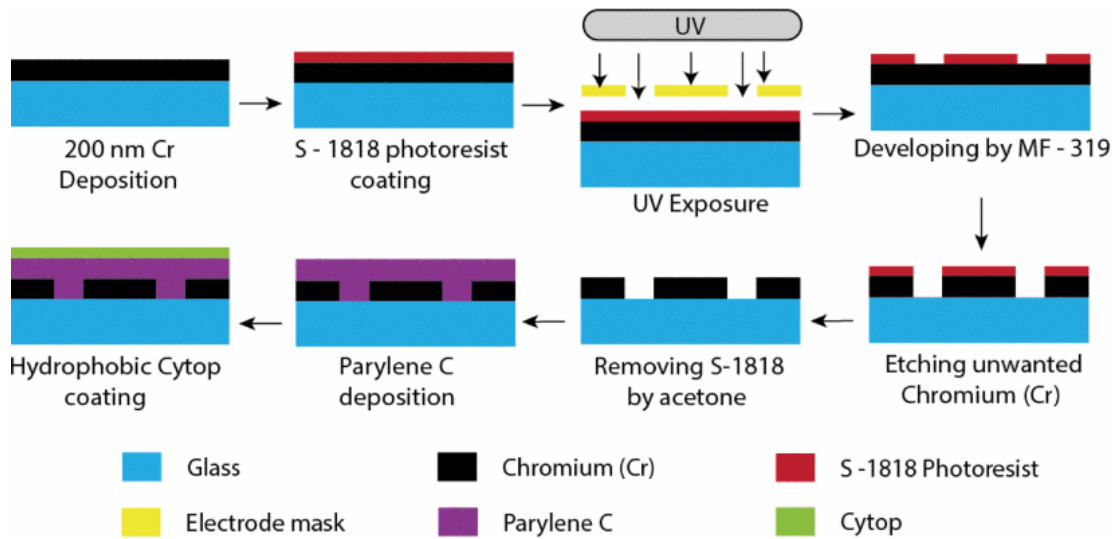
**Figure 3** Side-view schematics of: (a) one-plate- and (b) two-plate DMF devices.

### 1.1.2 Fabrication and implementation

A DMF device, in two-plate configuration, consists of four components: substrate, electrodes, dielectric layer, and hydrophobic layer (Figure 3b). Proper selection of these components is critical, as it determines the complexity and cost of the applicable fabrication methods used for the manufacturing of DMF devices. The substrate containing the

electrodes (bottom plate) is usually fabricated by photolithography and wet etching under cleanroom conditions (Figure 4a). These microfabricated bottom plates consist of metal electrodes (chromium, gold, copper, or aluminium) patterned onto a glass substrate, which serves as actuation electrodes, controlled by external voltage supplies. On the other hand, the top plate is usually an ITO-coated glass slide that serves as a continuous ground electrode. Both the ITO-coated top plate and dielectric-coated bottom plate are typically coated with a sub-micron-thick hydrophobic layer of fluoropolymers, such as Teflon<sup>®</sup> and FluoroPel<sup>®</sup>, to avoid the sticking of the sample droplets.

**(a) Fabrication of DMF devices by photolithography and wet etching**



**(b) Fabrication of DMF devices by inkjet printing**

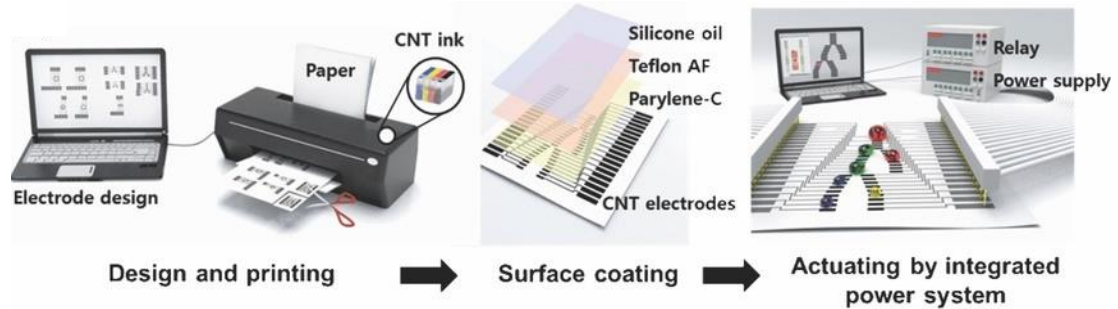


**Figure 4** Schematics of DMF bottom plate fabrication (examples from literature) by: **(a)** Photolithography and wet etching; reprinted with permission from ref. [26], © 2017 by IEEE, and **(b)** Inkjet printing; modified and reprinted with permission from ref. [27], © 2014 by WILEY-VCH Verlag GmbH & Co. KGaA, Weinheim

Recently, there have been developments in cleanroom-free techniques to fabricate DMF devices, such as microcontact printing,<sup>[28]</sup> PCB manufacturing,<sup>[29]</sup> and inkjet printing<sup>[30]</sup> (Figure 4b), which allows for the on-demand customization of electrode arrays for the rapid prototyping of new device designs.

The choice of dielectric material in DMF is crucial, as it affects the driving force (F) experienced by a droplet upon actuation, which is given by the following electromechanical equation,<sup>[12]</sup>

$$F = \frac{L}{2} \left( \sum_i \frac{\epsilon_0 \epsilon_{ri,liquid} V_{i,liquid}^2 (j2\pi f)}{d_i} - \sum_i \frac{\epsilon_0 \epsilon_{ri,filler} V_{i,filler}^2 (j2\pi f)}{d_i} \right) \quad (1)$$

where  $L$  is side of the cross-sectional area of the droplet, approximated as a square;  $f$  is the operating frequency;  $\epsilon_0$  is the permittivity of free space;  $\epsilon_{ri,liquid}$ ,  $V_{i,liquid}$  and  $\epsilon_{ri,filler}$ ,  $V_{i,filler}$  are the relative permittivity and voltage drop for the liquid and filler fluid portions of the electrode, respectively; and  $d_i$  is the thickness of layer  $i$ . The subscript  $i$  represents one of the dielectric, top and bottom hydrophobic, and liquid/filler layers. From Equation (1), it is clear that the driving force of a droplet is dependent on the relative permittivity or dielectric constant and the thickness of the dielectric material. Therefore, a material with a high dielectric constant that can be coated as a thin film in few-micrometer-thickness is generally favored as a dielectric.<sup>[31]</sup> The most commonly used dielectric material in DMF is Parylene C due to its high dielectric constant and defect-free coating by chemical vapor deposition (CVD). Due to the relatively high cost of CVD instrumentation, spin-coatable polymers, such as SU-8, have also been used as an inexpensive alternative.<sup>[32,33]</sup> There are also other non-cleanroom dielectric materials, such as polyimide or PDMS, that can be coated via lamination and spin coating,<sup>[34]</sup> as well as cyanoethyl pullulan, that can be roll-coated on inkjet-printed devices.<sup>[35]</sup>

The fluidic operations on DMF are carried out by applying a series of voltages across the array of electrodes, and the series can be programmed via automation systems without any manual intervention. Recent releases of open source automation systems, such as DropBot<sup>[36]</sup> and OpenDrop,<sup>[37]</sup> have made automated DMF technology available for everyone.

### 1.1.3 Detection

In terms of analyzing the samples, DMF has been integrated with a wide variety of analytical systems for both on- and off-line analysis. The most commonly used analytical methods in DMF for *in situ* detection of analytes are optical, electrochemical, and mass spectrometric detection. Using optical systems in addition to DMF, fluorescence from immunoassays or cells,<sup>[38]</sup> absorbance from bacterial or algae culture,<sup>[39]</sup> and chemiluminescence<sup>[40]</sup> from immunoassays have been monitored on-line. To detect electrically active analytes, electrochemical (EC) electrodes have been integrated on the DMF substrate along with sample actuation electrodes. This allows for the on-line analysis of samples via voltammetry,<sup>[41]</sup> amperometry,<sup>[42]</sup> and impedance<sup>[43]</sup> based EC measurements. For non-targeted analysis and proteomics applications, DMF-based sample preparation has been integrated with mass spectrometry (MS).<sup>[44]</sup> Moreover, samples have been analyzed either off-line directly on the surfaces via matrix-assisted laser desorption ionization (MALDI)<sup>[45,46]</sup> and nanostructure-initiator mass spectrometry (NIMS)<sup>[46]</sup> or on-line via an integrated electrospray ionization (ESI) emitter.<sup>[47]</sup> In rare cases, DMF has also been

integrated with channel microfluidics for the on-line separation of multiple analytes or products prior to analysis,<sup>[48,49]</sup> and with droplet microfluidics device for single-cell assays<sup>[50]</sup> and yeast cell sorting.<sup>[51]</sup> There have also been several attempts to integrate DMF with surface plasmon resonance (SPR) for imaging DNA hybridization<sup>[52]</sup> and with NMR for the detection of small- and bio-molecules.<sup>[53]</sup>

#### 1.1.4 Advantages and current challenges of DMF in chemical biology

Due to its versatility and reduced consumption of expensive reagents, DMF has been extensively used in a variety of applications in chemical biology.<sup>[17]</sup> These applications include, but are not limited to, chemical synthesis,<sup>[54,55]</sup> enzymatic reactions,<sup>[56,57]</sup> immunoassays,<sup>[38,40,58]</sup> proteomics,<sup>[59,60]</sup> biopsy<sup>[61,62]</sup>-, nucleic acid<sup>[63–65]</sup>-, and cell<sup>[66–68]</sup> based assays. The advantages of DMF over similar conventional counterpart technology in these applications are reviewed in Table 1.

**Table 1** *Examples of advantages associated with the use of DMF in a variety of applications, when compared with conventional methods. Modified and reprinted with permission from ref. [69], © 2016 by Elsevier.*

<b>Applications</b>	<b>Examples of advantages of using DMF-based methods in lab-on-a-chip applications</b>
<b>Chemical Synthesis</b>	–Automation and speed in the synthesis of compounds <sup>[54], [55]</sup>
<b>Enzymatic Reactions</b>	–Automation and speed, allowing studies of fast reaction kinetics not achievable before <sup>[56]</sup> –DMF allowed the first step in the development of a biomimetic Golgi <sup>[57]</sup>
<b>Immunoassays</b>	–Decrease in sample amount (by 100 times) <sup>[38]</sup> –Speed (10 times faster) <sup>[38]</sup> –Portability <sup>[58]</sup>
<b>Nucleic Acids</b>	–Reduction in sample amount (by ~5 times) <sup>[63]</sup> –Reduction in time for PCR amplification (by 50%) <sup>[64]</sup> –Improvement in detection limit (by ~100 times) <sup>[65]</sup>
<b>Proteins</b>	–Elimination of centrifugation for processing <sup>[59]</sup> –Significant reduction in protein processing analysis (from ~12 h to 30 min) <sup>[60]</sup>
<b>Cells, and Multicellular Organisms</b>	–Increase in sensitivity (~20 times) <sup>[66]</sup> –Speed and reduced shear stress in cells, in cell signaling studies <sup>[67]</sup> –Automation <sup>[68]</sup>

In spite of the aforementioned benefits, there are some challenges in implementing DMF in biological applications. These challenges can be both fundamental (such as biofouling and sample evaporation) and technical (such as limited throughput, temperature control, and DMF-to-world interfacing). The critical challenge when using DMF for analysis of proteins

and other large biomolecules is their non-specific adsorption (i.e., biofouling) onto the device surfaces. The commonly used hydrophobic coatings, such as Teflon<sup>®</sup> or FluoroPel<sup>®</sup>, are somewhat porous and retain proteins and other hydrophobic molecules nonspecifically.<sup>[70]</sup> To avoid the biofouling and subsequent cross-contamination between samples, surfactants such as Pluronic<sup>®</sup>, are typically added to the sample droplets to increase the device's longevity and reliability.<sup>[71]</sup> The use of surfactants may however impact, for instance, the enzyme activities,<sup>[72,73]</sup> which should be considered while selecting a suitable surfactant for the reaction. Biofouling may also impact the programmed sequences (automated assays) if the sample droplet sticks onto an electrode and does not move to the next destination. To overcome such issues, image based feedback systems can be used to optically sense the position of the stuck droplet, after which a control algorithm is executed for re-routing the droplet path until it reaches the destination electrode.<sup>[74]</sup> Sample evaporation is usually more of a challenge on one-plate than two-plate devices, especially if the assay protocols are longer than few seconds–minutes. In two-plate devices, the sample evaporation becomes significant when the devices are heated to higher temperatures for longer periods of time. This can be overcome by either using an oil-medium or replenishing the reaction volume with droplets of solvents in air-matrix devices.<sup>[75]</sup>

With respect to technical challenges, DMF platforms are usually medium throughput systems. The throughput may however be scaled up by increasing the number of DMF actuation electrodes, although that simultaneously also increases the lateral dimensions of the device. To minimize the number of electrodes needed for actuation of droplets in a reaction, more focus is needed in physical design. While designing the electrode arrays, efficient routing should be considered between different reactors/modules, and also between individual reactors/modules and the input/output reservoirs and thus to be able to perform as many as possible parallel operations.<sup>[76]</sup>

Even though the use of DMF in bio-chemical and immunological assays has been well-established, the feasibility of DMF technology for drug discovery and development is seldom explored, with a few exceptions. For example, Jabriel et al. explored the feasibility of two-plate DMF for high-throughput drug synthesis and screening by demonstrating the on-chip parallel synthesis of five different macrocycles<sup>[55]</sup> and combinatorial synthesis of four different peptidomimetics.<sup>[77]</sup> In another work by Au et al., hepatic organoids were cultured to perform drug screenings on a DMF platform.<sup>[78]</sup> A field that has not attracted much interest prior to this thesis work is the implementation of droplet-based drug metabolism assays on DMF devices. Drug metabolism per se is one of the corner stones of preclinical ADME screening of new drug candidates and could largely benefit from miniaturization. Although DMF devices are relatively mature for droplet-based sample preparation in general, as reviewed in Table 1, the aforementioned hurdles or development needs limit the implementation of enzyme-mediated drug metabolism assays on DMF. First critical requirement is the precision of the world-to-DMF interfacing, i.e., the way in which the samples are introduced for chemical and biological reactions in a quantitative and automated manner.<sup>[79,80]</sup> A second rarely addressed point of development is DMF-to-world interfacing, i.e., the way in which the samples from DMF reactions are processed further if the *in situ* detection is not sufficiently selective.<sup>[48,49,80]</sup> In case of drug metabolism, it is typically desirable to separate the drug metabolites from the parent drug and possible cosubstrates prior to their detection. Even though few attempts have been made with respect

to sample separation, as mentioned in the previous section (1.1.3), this aspect is not thoroughly established likely due to the differences in the applicable microfabrication materials and methods. Finally, precise, localized temperature control of DMF devices is another critical requirement for enzymatic reactions. Many of the biological applications are conducted by placing the chip in a heated incubator.<sup>[81]</sup> Although there has been some development recently with respect to integration of on-chip temperature control using heating blocks or commercial heating elements.<sup>[79,80]</sup>

## 1.2 Significance of metabolism to safety and efficacy of drugs

CYP-mediated drug metabolism studies are important to (i) make predictions of the drug clearance *in vivo* based on metabolic clearance rates determined *in vitro* (which will be discussed in Section 1.2.1) and (ii) evaluate drug clearance *in vivo* from patient samples, such as blood, urine, and tissue biopsy (Section 1.2.2).

### 1.2.1 Role in pre-clinical drug development *in vitro*

Drug metabolism involves the transformation of drugs, xenobiotics, and other endogenous molecules, such as steroids and hormones, by specialized enzyme systems, primarily in the liver. Among the drug metabolizing enzymes, the CYP superfamily is responsible for metabolism of the majority of drugs and several other xenobiotics. The CYP superfamily consists of 18 families (CYP1, 2, etc.) and 44 subfamilies (1A, 2B, etc.).<sup>[82]</sup> Among those, families CYP 1–3 are primarily responsible for the metabolism of the majority of drugs, totaling 70–80% of marketed pharmaceuticals,<sup>[5,6,83]</sup> as well as other drug-like xenobiotics, e.g., procarcinogens.<sup>[84]</sup> To assess the safety and efficacy of new drug candidates, the metabolic clearance rate and identification of both the metabolites produced and the CYP isoenzymes responsible for their elimination should be carefully studied and examined.<sup>[85]</sup> Although both computational methodologies and nonenzymatic techniques (such as electrochemical oxidation or titanium dioxide induced photocatalysis<sup>[86]</sup>) are available, mimicking the selectivity of enzymatic reactions is still challenging to both of these methods. Therefore, enzymatic screening of new drug candidates *in vitro* is vital in the drug discovery process. The most commonly used matrices in the assessment of human drug metabolism are recombinant CYP enzymes (rCYP), human liver microsomes (HLM), and human primary hepatocytes. rCYPs expressed in insect cells are used for the preliminary screening of the isoenzymes in charge of the drug candidates' metabolism.<sup>[87]</sup> HLMs are vesicle artifacts of the endoplasmic reticulum of liver cells prepared from the donor's liver tissues (from deceased donors) for the preliminary *in vitro* estimation of the metabolic clearance.<sup>[88]</sup> Hepatocytes are also used for the above mentioned *in vitro* assessments, except that these better take into account the full complexity of the cellular scale, including drug transport into the cell and metabolite transport out of the cell.<sup>[89]</sup> In addition to these matrices and models, metabolic clearance rates are also assessed from biological fluids (blood, urine) during clinical trials and post-marketing studies.<sup>[90]</sup>



## 1.2.2 Role in drug dosing

The metabolic activity of some CYP isoenzymes varies between individuals based on genetic variations (polymorphisms) and other external factors, such as age, sex, diet, medication, disease condition, and exposure to chemicals.<sup>[5]</sup> This inter-individual variation in drug metabolism plays a vital role in the safety and efficacy of treatment, as the drug clearance rate is directly correlated with drug concentrations in the blood. Low metabolic activity causes increased blood levels, which may lead to toxic or other severe adverse effects. However, rapid metabolism causes reduced blood levels, which may lead to inefficacy. The most important drug metabolizing CYP enzymes and the primary factors affecting their expression in the liver are given in Figure 5.

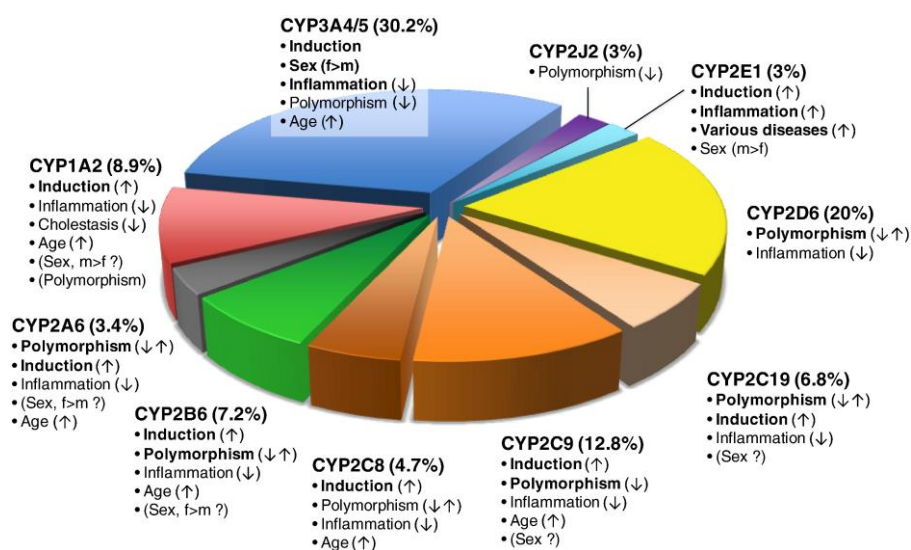


**Figure 5** Fractions of the clinically used drugs metabolized by P450 enzymes and factors influencing variability, which are indicated by bold type with possible directions of influence indicated (↑, increased activity; ↓, decreased activity; ↑↓, increased and decreased activity). Factors of uncertain significance are shown in parentheses. Reprinted from ref. [5], © 2013 by Zanger et al.; Elsevier, CC BY-NC-ND 4.0.

To predict polymorphism based variation in CYP activity, genetic tests exist for specific CYP isoenzymes that are known to be polymorphic (for CYP2C9 and 2D6);<sup>[91]</sup> however, these tests are not capable of predicting the variation arising from external factors. Therefore, it is more relevant to measure the *in vivo* CYP activity in the liver, for example in the context of biopsying, especially when designing the medical therapy of critically-ill patients suffering from cancer, liver diseases, chronic depression, etc. In this study, focus was put on the CYP1A1 activity. The activity and regulation of CYP1A1 is responsible for the metabolism of several anti-cancer drugs and carcinogenic substances that vary significantly based on several non-genetic factors.<sup>[92]</sup> Environmental exposure to heavy metals increases the levels of CYP1A1 due to oxidative stress,<sup>[93]</sup> while exposure to pesticides inhibits the activity of CYP1A1/2.<sup>[94]</sup> Furthermore, life-style choices, such as smoking, is found to affect the CYP1A1 metabolism of anti-cancer drugs, such as erlotinib, for which the area under the curve (AUC) is 2.8 times lower than that of non-smokers.<sup>[95]</sup>

Therefore, assessing the CYP activity of individuals requiring life-saving medication would radically improve the safety and efficacy of treatment by precision dosing.

### 1.2.3 Miniaturization of drug metabolism assays

Ever since the introduction of the  $\mu$ TAS concept, there has been a constant development of new microfluidic technologies for both drug discovery and clinical analysis purposes to reduce the consumption of expensive reagents and to spare the limited clinical samples via miniaturization. Miniaturized/microfluidic systems provide rapid and parallel analysis with improved analytical performance through multiplexing and automation.<sup>[96]</sup> Thus, microfluidics technology has been used for various aspects, such as drug synthesis,<sup>[11]</sup> drug screening,<sup>[97]</sup> drug metabolism,<sup>[98]</sup> and drug toxicity screening *in vitro*,<sup>[99]</sup> as reviewed in Figure 6. Concerning drug metabolism research specifically, the focus has been on the implementation of: (i) immobilized enzyme (micro)reactors (IMERs) using recombinant enzymes or HLM to assess drug-drug interactions<sup>[100]</sup> and (ii) organ-on-a-chip models to assess drug metabolism on a cell/tissue level.<sup>[101]</sup> In the IMERs, CYP enzymes are often immobilized on channel walls or high-surface-area structures, such as micropillars, monoliths, and microbeads<sup>[102]</sup> and can be further integrated with separation and detection units.<sup>[103]</sup> Enzyme immobilization improves the stability of the enzymes, as well as the separation of the reaction solution from the enzymes after the reaction, which facilitates the subsequent detection of metabolites.<sup>[104,105]</sup> There are also other miniaturized systems that exist, such as lateral flow paper-based assays, where CYP enzymes are immobilized on functionalized paper substrate to assess metabolic clearance<sup>[106]</sup> and 1134 parallel microarrays of nanoliter-scale gel compartments encapsulating CYPs patterned on functionalized glass substrates for high throughput CYP assays.<sup>[104]</sup> Contrary to sub-cellular models, which often focus on mechanism-based drug metabolism studies, the organ-on-a-chip models are most often used for prediction of system level toxicity associated with drugs and their metabolites.<sup>[107]</sup>

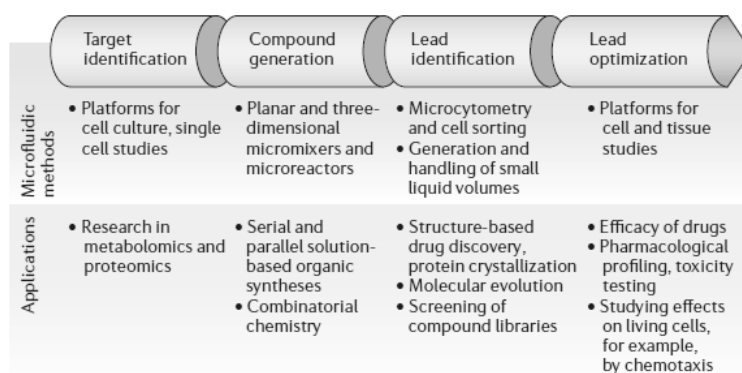


**Figure 6** *Microfluidic methods and their respective applications during the different steps of drug discovery. Reprinted with permission from ref. [11], © 2006 by Springer Nature.*

Although microfluidics in its various forms has been extensively applied to drug discovery and development, and DMF has been well-established in various biological applications, the potential of DMF in drug metabolism research has not been specifically and comprehensively studied before this work. This is likely due to the development needs associated with DMF devices, as discussed in chapter 1.1.4, as well as the complexity of the CYP system, which includes multiple cofactors, needing to be maintained at physiological temperature and having inherently low metabolite yields. In this thesis, CYP metabolism assays were implemented on a DMF platform in droplet-scale by thoroughly addressing the fundamental and technical challenges associated with the DMF-based enzyme assays.

## 2 Aims of the study

The overall aim of the study was to implement drug metabolism assays on digital microfluidics (DMF) technology in droplet-scale to address the real-world needs of both preclinical drug development and the clinical assessment of metabolic clearance from patient samples. This was addressed by bridging the technological gaps w.r.t. thermal control of the DMF devices, and DMF-to-world interfacing by introducing new materials that facilitate sensitive detection of low-yield CYP metabolites by optical and mass spectrometric methods and DMF interfacing with channel microfluidics to further improve the detection selectivity. Another fundamental aim was to develop low-cost, cleanroom-free, bench-top fabrication methods and interfaces that can be adapted to routine use in standard laboratory conditions and thereby promoting the development of DMF-based bioanalytical platforms in general.

More detailed aims include:

- to select and examine DMF dielectric materials suitable for *in situ* optical and mass spectrometry detection of low-yield CYP metabolites on-chip
- to examine the possibility of integrating DMF with channel microfluidics via inkjet-printing and using thiol-enes to fabricate the dielectric layer as well as the microchannel unit
- to examine the recreation of physiological conditions on-chip by developing a microheater-element for localized temperature control to maintain maximum enzyme activity
- to examine the feasibility of different solid support materials for CYP immobilization for droplet-scale drug metabolism studies on DMF platforms
- to examine the feasibility of fluorescent probes for quantitation of the metabolic clearances via different CYP enzymes
- to examine the possibility of ambient MS for *in situ* identification of the metabolite
- to evaluate the feasibility of DMF-based droplet microreactors for the determination of patient-to-patient variation in CYP activities

### 3 Materials, instrumentation and standard methods

This chapter contains the list of chemicals, materials, and instruments used in the study in Section 3.1, while protocols of standard methods and off-chip control experiments are described in Section 3.2.

#### 3.1 Chemicals, microfabrication materials and instrumentation

The chemicals/reagents, solvents and enzymes used in this study are listed in Table 2, microfabrication materials in Table 3, and instrumentation and software in Table 4. The column “Note” indicates their purposes.

**Table 2** *Chemicals and reagents used in the study*

Reagents/materials	Manufacturer/supplier	Note	Publication
Acetone, Chloroform	Sigma-Aldrich, Germany	Solvents	I, II, IV
Methanol	Sigma-Aldrich, Germany	Solvent	I-III
Ethylene glycol, Octonal	Sigma-Aldrich, Germany	Solvents	I, II
Dimethyl sulfoxide	Sigma-Aldrich, Germany	Solvent	I-IV
Isopropyl alcohol	Sigma-Aldrich, Germany	Solvent	III
Trifluoroacetic acid	Riedel-de Haen, Germany	Reagent	II
Milli-Q Water	Millipore, France	Solvent	I-IV
Magnesium chloride	Sigma-Aldrich, Germany	Reagent	I, II, IV
Phosphate buffer saline (PBS)	Sigma-Aldrich, Germany	Buffer	I, II, IV
Ammonium hydroxide	Riedel-de Haen, Germany	Reagent	
Dipotassium hydrogen phosphate	Amresco, OH	Buffer salt	I, II, IV
Potassium dihydrogen phosphate	Riedel-de Haen, Germany	Buffer salt	I, II, IV
Rhodamine B	Sigma-Aldrich, Germany	Reagent	I, II
Naproxen, Paracetamol, Carbamazepine	Sigma-Aldrich, Germany	Drugs	II
Testosterone	Sigma-Aldrich, Germany	Standard	II
Trizma® base	Sigma-Aldrich, Germany	Buffer	II, IV
Biotin-PEG4-alkyne	Sigma-Aldrich, Germany	Reagent	I, II
Alexa Fluor® 488 streptavidin conjugate	Thermo Fisher Scientific, MA	Reagent	I, II
7-ethoxy resorufin	Toronto Research Chemicals, Canada	Reagent	I, IV
Dibenzylfluorescein	Organix Inc., MA	Reagent	IV
Resorufin	Sigma-Aldrich, Germany	Reagent	I, IV
Recombinant enzymes (CYP1A1, 1A2)	Corning, Germany	Enzyme product	I, II

Human liver microsomes	Corning, Germany	Enzyme product	IV
3-Cyano-7-ethoxycoumarin (CEC), Cyano-umbelliferone (CHC), Coumarin, Umbelliferone, Fluorescein	Sigma-Aldrich, Germany	Reagents	IV
$\beta$ -nicotinamide adenine dinucleotide 2'-phosphate reduced tetrasodium salt hydrate (NADPH)	Sigma-Aldrich, Germany	Reagent	I, II, IV
Pluronic F-68	Sigma-Aldrich, Germany	Reagent	I-IV
Dynabeads® M-280 Streptavidin beads	Invitrogen, Norway	Magnetic beads	IV
1,2-dioleoyl-sn-glycero-3-phosphoethanolamine (DOPE); 1,2-dioleoyl-3-trimethylammonium-propane (chloride salt) (DOTAP); 1,2-dioleoyl-sn-glycero-3-phosphoethanolamine-N-(Cap biotinyl) (sodium salt) (biotin-DOPE); 1,2-dioleoyl-sn-glycero-3-phosphoethanolamine-N-(lissamine rhodamine B sulfonyl) (ammonium salt) (Liss-Rhod PE)	Avanti Polar Lipids, AL	Lipids	I, II, IV

**Table 3** *Microfabrication materials used in the study*

Materials	Manufacturer/supplier	Note	Publication
Pentaerythritol tetrakis(3-mercaptopropionate), > 95% (tetrathiol); 1,3,5-triallyl-1,3,5-triazine-2,4,6(1H,3H,5H)-trione, 98% (triallyl)	Sigma-Aldrich, Germany	Dielectric, monolith	I-IV
Irgacure® TPO-L	BASF, Germany	Photoinitiator	I-IV
SU-8 5	Microchem Corp., MA	Dielectric	I-III
SU-8 25	Microchem Corp., MA	Dielectric	III
SU-8 100	Microchem Corp., MA	Master	III
Slygard 184 base elastomer (PDMS) and curing agent	Dow chemical company, MI	Mold	III
Fluorpel® PFC 1604V and PFC 110 solvent	Cytonix LLC, MD	Hydrophobic coating	I-IV
Chrome-etchant 3144 Puranal	Honeywell International, NJ	Etchant	I, II, IV
AZ 351B resist developer	MicroChemicals GmbH, Germany	Developer	I, II, IV

Novele IJ-220 printing media, Metalon JS-B25P silver nanoparticle ink and Melton Aqueous Vehicle (solvent)	NovaCentrix, TX	DMF and microheater	III, IV
AGIC-CP01A4 special coated paper and AGIC-AN01 silver nano ink	AgIC Inc., Japan	Microheater	I, II
Sodalime glass coated with chromium and Az 1500	Telic company, CA	Bottom plate	I, II, IV
Indium tin oxide coated glass slide	Structure Probe Inc., PA	Top plate	I, II, IV
Silicon wafers	Siegert wafer, Germany	Master	IV
Plastic photomasks	Micro Lithography services, UK	Patterning	I-IV
ITO-PET film	MEMCON Ltd., MI	Top plate	IV

**Table 4** *Instruments and softwares used in the study*

Instrumentation/software	Manufacturer/supplier	Publication
<b>For microfabrication</b>		
Laurell Spin coater WS-650Mz-23NPPB	Laurell Technologies Corporation, PA	I-IV
Dymax 5000-EC series UV flood exposure lamp	Dymax Corporation, CT	I-IV
DropBot DMF automation system, controlled by MicroDrop v2.4 software	Open source (built in-house)	I-IV
FEI Quanta™ FEG scanning electron microscope	FEI company, OG	I, IV
Brother MFC-J5910DW inkjet printer	Brother Industries, Ltd., Japan	I, II
AutoCAD 2015 software	Autodesk Inc., CA	I-IV
ImageJ image analysis software	National Institute of Health, MD	I
<b>For microheater fabrication and characterization</b>		
Epson C88+ inkjet printer	Seiko Epson Corporation, Japan	II, IV
CHAL-002 miniature thermocouple	OMEGA Engineering, UK	I, IV
Fluke 289 multimeter	Fluke Corp., WA	I, IV
FLIR A325sc IR camera	FLIR Systems, WA	I
Retiga 4000R digital microscope camera	QImaging, Canada	I
<b>For analytical methods</b>		
Zeiss Axioscope A1 upright epifluorescence microscope <sup>a</sup>	Zeiss Finland Oy, Finland	I, III, IV
Varioskan LUX multimode well-plate reader	Thermo Fisher Scientific, MA	I, IV
Bruker micrOTOF™ mass spectrometer and Compass DataAnalysis 4.0 software	Bruker Daltonics, Germany	II
Krypton filled PKR 106 V-UV lamp	Heraeus Noblelight GmbH, Germany	II
Programmable HV supply	Custom built	IV

PicoScope 2203 AD converter with PicoLog recorder	Pico Technology, UK	IV
---	---------------------	----

<sup>a</sup> Equipped with HAL 100 (100 W) halogen lamp as excitation source with bandpass excitation (546±6 nm) and emission (488-640 nm) filters.

## 3.2 Standard methods and protocols

### ***Biotinylation of recombinant enzymes and human liver microsomes***

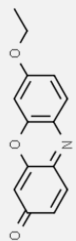
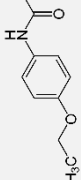
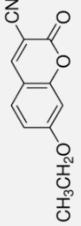
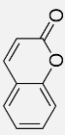
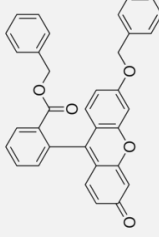
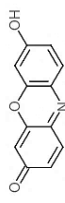
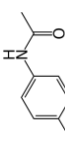
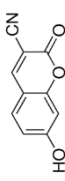
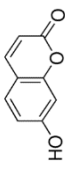
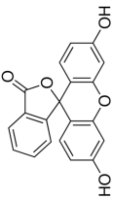
The biotinylated fusogenic liposomes were prepared as described in reference.<sup>[108]</sup> The lipids DOPE, DOTAP, biotin-DOPE, and Liss-Rhod PE were dissolved in chloroform and mixed in the ratio of 1:1:0.1:0.05 (*wt*-%, 1 mg of total lipid content), while the solvent was evaporated to dryness for ca. 2 h in a vacuum desiccator. Next, 1000 µL of PBS buffer was added and the re-solubilized lipid mixture was vortexed at RT for 1 h to form multilamellar liposomes. The multilamellar liposomes were extruded through a 0.1 µm filter 51 times to form biotinylated unilamellar vesicles. The biotinylated unilamellar vesicles were then fused with either human recombinant CYP enzymes (rCYP, 1000 pmol/mL) expressed in insect cells in Publications I and II or with HLMs (20 mg/mL), the vesicle-like artifacts of the ER incorporating membrane-bound CYP (prepared via centrifugation) in Publication IV in a volumetric ratio of 1:1, at 37 °C for 15 min.

### ***Control enzyme incubations***

The off-chip control incubations in Publication IV were carried out with soluble- and immobilized (on magnetic beads) HLM in 100 µL volume in microtubes. The reaction solution consisted of the chosen model substrate (Table 5) and cosubstrate (1 mM NADPH) in a suitable buffer. The chosen substrates were isoenzyme specific, low, or non-fluorescent and known to produce fluorescent metabolites. In the case of soluble enzyme reactions, 0.8 mg/mL (total protein) of HLMs were used, whereas in immobilized enzyme assays, 0.25 mg of beads (incorporating the immobilized HLM) were added to the reaction volume. The solutions were incubated at 37 °C with a commercial heating block and the detailed incubation conditions are given in Table 6. After incubation, the soluble enzyme reactions were terminated by adding an appropriate termination solution (Table 6), placing a microtube in an ice bath for 15 min, and centrifuging at 16000 *g* for 10 min. Thereafter, the supernatant was collected for further analysis. The immobilized enzyme reactions on beads were terminated by separating the magnetic beads with the help of a magnet and collecting the supernatant. In both cases, the supernatant was analyzed for fluorescence (originating from the metabolites) with a wellplate reader.



**Table 5** Incubation conditions of CYP assays

	CYP1A1	CYP1A2		CYP2A6	CYP3A4
Substrate	 7-ethoxyresorufin (2 $\mu$ M)	 Phenacetin (100 $\mu$ M)	 CEC (4 $\mu$ M)	 Coumarin (30 $\mu$ M)	 DBF (4 $\mu$ M)
Metabolite	 Resorufin	 Paracetamol	 CHC	 Umbelliferone	 Fluorescein
Reaction in solution with soluble enzymes (0.8 mg/mL)					
Buffer	Phosphate	N/A	Tris	Tris	Tris
Time (min)	30	N/A	20	20	20
Quenching	2 M NaOH (10%-vol)	N/A	ACN	4 M Perchloric acid (10%-vol)	2 M NaOH (10%-vol)
Ex/em (nm)	570/590	N/A	413/454	325/477	496/516
Reaction in solution with immobilized enzymes (on magnetic beads)					
Buffer	Phosphate	N/A	Tris	Tris	Tris
Time (min)	30	N/A	30	30	30
Ex/em (nm)	570/590	N/A	410/453	331/460	495/516
Reaction in DMF devices (30 min incubation)					
Buffer	Phosphate	15 mM Tris	Tris	Tris	Tris
Ex/em (nm)	570/590	N/A	410/453	331/460	495/516

CEC: 3-cyano-7-ethoxycoumarin; CHC: 3-cyanoumbelliferone; DBF: dibenzylfluorescein; Phosphate: 0.1 M potassium phosphate (pH 7.4) with 5mM MgCl<sub>2</sub>; Tris: 0.1 M Tris (pH 7.4); ACN: 40% of reaction volume of acetonitrile:0.5 M Tris-base (80:20); 10%-vol: 10% of reaction volume; N/A: not applicable. Probes recommended by FDA are written in italics.

## 4 Experimental methods developed in the thesis

This chapter consists of the experimental methods and protocols developed in this thesis. This includes fabrication processes of DMF microchips and microheaters, functionalization protocols for the immobilization of CYP enzymes on solid supports, operation protocols of on-chip assays, and protocols for integrating DMF devices with microchannel for electrophoresis and detection methods for on-chip analysis of metabolites by fluorescence or ambient mass spectrometry.

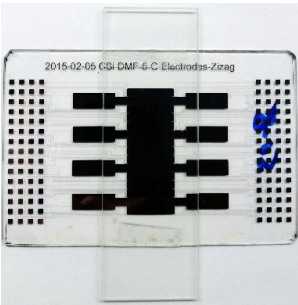
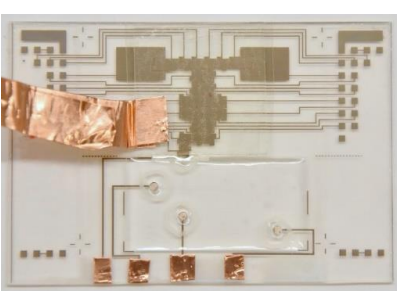
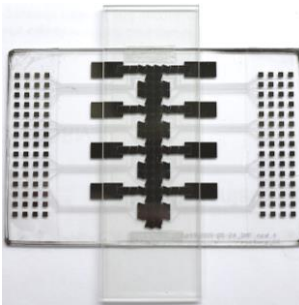
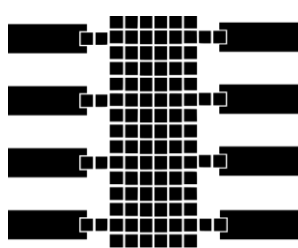
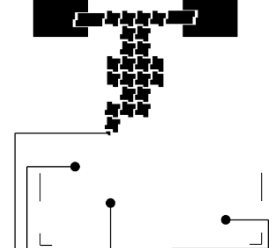
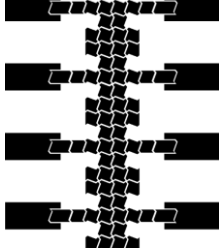
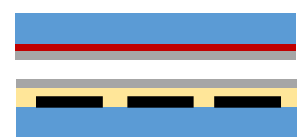
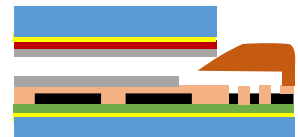
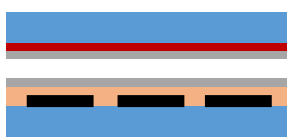
### 4.1 Microchip designs, fabrication and operation

Two types of DMF devices were developed and used in this study: (i) glass-based DMF devices for drug metabolism and distribution assays in Publications I, II and IV; and (ii) inkjet-printed DMF devices for interfacing with microchannel in Publication III. The electrodes and microchannel layouts of the devices were designed using AutoCAD, while the devices were fabricated, assembled, and operated in cleanroom-free laboratory conditions. Expensive and time-consuming cleanroom fabrication was avoided by using commercial glass substrates pre-coated with chromium and AZ resist and inkjet printing for fabricating the DMF electrodes and microheaters on the flexible polymer sheets. In all subprojects, SU-8 or thiol-ene polymers were used as dielectric materials because of their relatively low-cost and simple fabrication via spin-coating and UV curing.

#### *Fabrication of glass-based DMF devices*

To fabricate the DMF electrodes, commercial glass substrate (50 mm × 75 mm) bearing chromium (100 nm) and AZ 1500 photoresist (530 nm) was patterned with UV exposure for 5 s through a plastic mask (commercial mask but designed in-house) bearing the electrode patterns. The substrate was then developed with AZ developer (20% in water v/v) for 20 s followed by chromium etching with chromium etchant for 45 s. After etching, the remaining resist was removed with acetone in an ultrasound bath (5 min). Prior to dielectric coating, the contact pads of the electrode arrays on both sides of the bottom plate were covered with dicing tape. An 8-μm-thick layer of SU-8 in Publications I and II, or thiol-ene in publication IV, were spin-coated and cured by UV exposure to serve as dielectric layers (Figure 7). The thiol-ene polymer was prepared from triallyl and tetrathiol monomers mixed in a stoichiometric ratio of functional groups. Finally, a sub-micron-thick fluoropolymer (1% Fluoropel®) layer was spin-coated onto the dielectric layers and cured by heating. The spin-coating, UV/heat curing, and baking (on a hot plate) processes were performed in a standard laboratory inside laminar fume hoods to avoid particle contamination. The critical fabrication parameters are given in Table 6. The top plate was fabricated by spin-coating the fluoropolymer onto an ITO-coated glass plate (25 mm × 75 mm), while the top- and bottom plates of the DMF were assembled using two layers of double-sided Scotch® tape as spacers, resulting in an inter-plate gap of ~180 μm.

DMF microchips used in the study

	Publication I & II	Publication III	Publication IV
Photograph of device			
Electrode layout			
Cross-section of device	 <ul style="list-style-type: none"> <li>Glass substrate</li> <li>SU-8 dielectric</li> <li>Actuation electrode</li> <li>ITO (ground)</li> <li>FluoroPel</li> </ul>	 <ul style="list-style-type: none"> <li>Glass support</li> <li>Thiol-ene dielectric</li> <li>Inkjet-printed Silver</li> <li>Thiol-ene microchannel device</li> <li>FluoroPel</li> <li>Novelle substrate</li> </ul>	 <ul style="list-style-type: none"> <li>Glass substrate</li> <li>Thiol-ene dielectric</li> <li>Actuation electrode</li> <li>ITO (ground)</li> <li>FluoroPel</li> </ul>

**Figure 7** Microchip designs used in this study: Top-view photographs of the fully-assembled devices, top-view CAD layout of electrodes on the bottom plate, and cross-section schematics of the fully-assembled devices.

**Table 6** Critical fabrication parameters of dielectric and hydrophobic coatings.

Material	Purpose	Spin coating parameters	UV curing	Baking	Publication
SU-8	Dielectric	1600 rpm, 30 s	15 s	65 °C, 2 min and 95 °C, 2 min <sup>a</sup>	I, II
Thiol-ene (1:1)	Dielectric	2000 rpm, 30 s	2 s	N/A	IV
Thiol-ene (1:1.25)	Dielectric	3000 rpm, 30 s	2 s	N/A	III
Fluoropel	Hydrophobic coating	1000 rpm, 30 s	N/A	150 °C, 30 min	I, II, IV
		1500 rpm, 30 s	N/A	150 °C, 30 min	III

<sup>a</sup> Both pre- and post exposure baking.

N/A=not applicable; thiol-ene compositions: 1:1=stoichiometric, 1:1.25=25% allyl excess.

## Fabrication of inkjet-printed DMF devices and microchannel interface

In Publication III, the DMF and MCE electrodes were patterned by printing silver nanoparticle ink onto a commercial, porous and flexible polymer substrate (Novele) using a commercial Epson inkjet printer. After printing, the substrate was heat-treated at 150 °C on a hot plate for 2 min to evaporate the residual solvent from the printed metallic ink. Each device pattern was then mounted on a glass plate using adhesive transfer tape, while the contact pads were covered with parafilm prior to the spin-coating of the dielectric layer on top of the printed electrodes. A 5- $\mu\text{m}$ -thick layer of thiol-ene polymer featuring 25% molar excess of allyl (ene) functional groups was spin-coated (Table 6) and cured with masked UV exposure in the non-contact mode for 2 s (Figure 8a). The photomask was used to expose the MCE electrodes and separated from the polymer layer with 0.15-mm-high spacers (Figure 8b). After exposure, the uncured thiol-ene was washed with methanol, which resulted in exposing the MCE electrodes. Finally, fluoropolymer was spin-coated and cured onto the thiol-ene dielectric by covering the microchannel (bottom) part of the substrate with parafilm while coating. The top part of the thiol-ene microchannel was fabricated by replica molding as described previously<sup>[109]</sup> and bonded onto the thiol-ene (Figure 8c), though not on the fluoropolymer coated DMF bottom plate, by manual lamination at 70 °C and cured under UV for 2 min.<sup>[110]</sup> The microchannel replication process included transferring the channel patterns first from an SU-8 master to a PDMS mold by soft lithography and then from PDMS to thiol-ene by UV-replica molding. The detailed fabrication protocols of the SU-8 master and PDMS mold are given in Publication III. The thiol-ene replica was prepared from a mixture with 25% excess allyl monomer poured onto the PDMS mold and cured with UV flood exposure for 5 min. The cured thiol-ene microchannel layer was carefully peeled off from the PDMS mold.

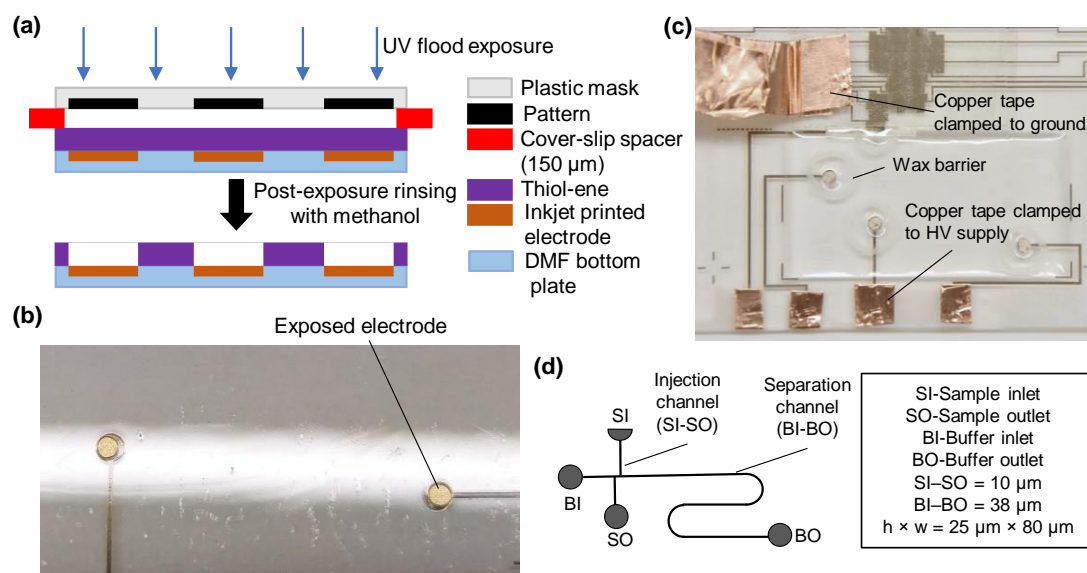


**Figure 8** (a) Side-view illustration of the thiol-ene coating on printed electrodes and their masked exposure. Photographs of (b) the exposed electrodes (dia = 1.6 mm) on thiol-ene coated bottom plate, and (c) thiol-ene microchannel bonded onto the bottom plate. (d) Design of the thiol-ene microchannel unit.

The microchannel design features a meandering pattern with dimensions of  $38\text{ mm} \times 25\text{ }\mu\text{m} \times 80\text{ }\mu\text{m}$  (length  $\times$  height  $\times$  width) and  $50\text{ }\mu\text{m}$  (width) tapering at the channel turns (Figure 5d). The design also features a double-T junction at the injection cross and  $\text{Ø}2\text{ mm}$  circular sample inlets/outlets. Hydrophobic wax barriers were drawn around the inlets of the microchannel using a wax pen to avoid leakage of the buffers and contacts between inlets under HV application. The contact pads of the MCE electrodes were covered with copper tapes before clamping to HV to avoid possible mechanical damage caused by the alligator clips.

An ITO-coated PET film ( $30\text{ mm} \times 30\text{ mm}$ ) laminated onto a glass slide using adhesive transfer tape and coated with fluoropolymer was used as the top plate. The top plate was assembled on the bottom plate with the flexible ITO-PET edge resting on top of the microchannel inlet (Figure 7). The top plate was grounded by clamping the grounded alligator clip to a flexible (conductive) copper tape affixed to the conductive side of the ITO-PET (Figure 8c).

### ***Droplet operations and characterization of dielectric properties***

The droplet operations on DMF devices were carried out with a DropBot open-source automation system<sup>[36]</sup> using MicroDrop software. Sample droplets were actuated by applying  $80\text{--}140\text{ V}_{\text{rms}}$  at  $10\text{ kHz}$  to the bottom plate electrodes, whereas the top plate was clamped to the ground. To actuate octanol droplets in drug distribution assays in Publication II, a lower frequency of  $300\text{ Hz}$  was used.

To characterize the thiol-ene dielectric in Publication III, unit droplets of water (with  $0.1\%$  *m/v* Tetronic 90R4 as the surfactant) were actuated back and forth with a normalized force of  $\sim 25\text{--}30\text{ }\mu\text{N/mm}$  with a DropBot controller, as described in the references.<sup>[35,111]</sup> Longevity of the devices were tested by actuating droplets in a circular path with a normalized force of  $25\text{ }\mu\text{N/mm}$  for 10 minutes, while the peak velocity at each step was measured.

## **4.2 Microheater fabrication and characterization**

The CYPs are sensitive to changes in temperature and their activities are at a maximum in a narrow temperature range close to the physiological temperature.<sup>[112]</sup> Therefore, the DMF device needed to be precisely and locally heated up to  $\sim 37\text{ }^{\circ}\text{C}$ . In Publications I, II and IV, inkjet printed microheaters were used for the localized heating of DMF devices. Integrated localized heaters provide better control over heating time and improved heat transfer efficiency compared to heating the entire device inside an incubator, as in cell-based applications.<sup>[81]</sup> All microheaters used in the study were fabricated by inkjet-printing conductive silver ink onto flexible substrate. The microheater design bears a meandering pattern made of  $200\text{-}\mu\text{m}$ -wide-lines covering a  $4\text{ mm} \times 4\text{ mm}$  area (equal to the area of four DMF electrodes) in Publications I and II, as well as four such meandering patterns in Publication IV to heat four reactions in parallel (Figure 9a). After printing, the heaters were heat treated at  $150\text{ }^{\circ}\text{C}$  for 2 min on a hot plate. The microheaters were assembled to the

bottom side of the DMF bottom plate with the help of a glass support and tape (Figure 9b). The temperature distribution across the heated DMF device was visualized with IR thermography, which is a fast and high resolution method for mapping the heat distribution across microfluidic devices.<sup>[113]</sup> IR thermographs were taken from the upper surface of the top plate. Figure 9c illustrates the local heating of the DMF device with a single heater, corresponding to an area of four actuation electrodes ( $4\text{ mm} \times 4\text{ mm}$ ), where the temperature was  $36\text{ }^{\circ}\text{C}$  (measured on the top plate), while the rest of the device was close to room temperature (RT).

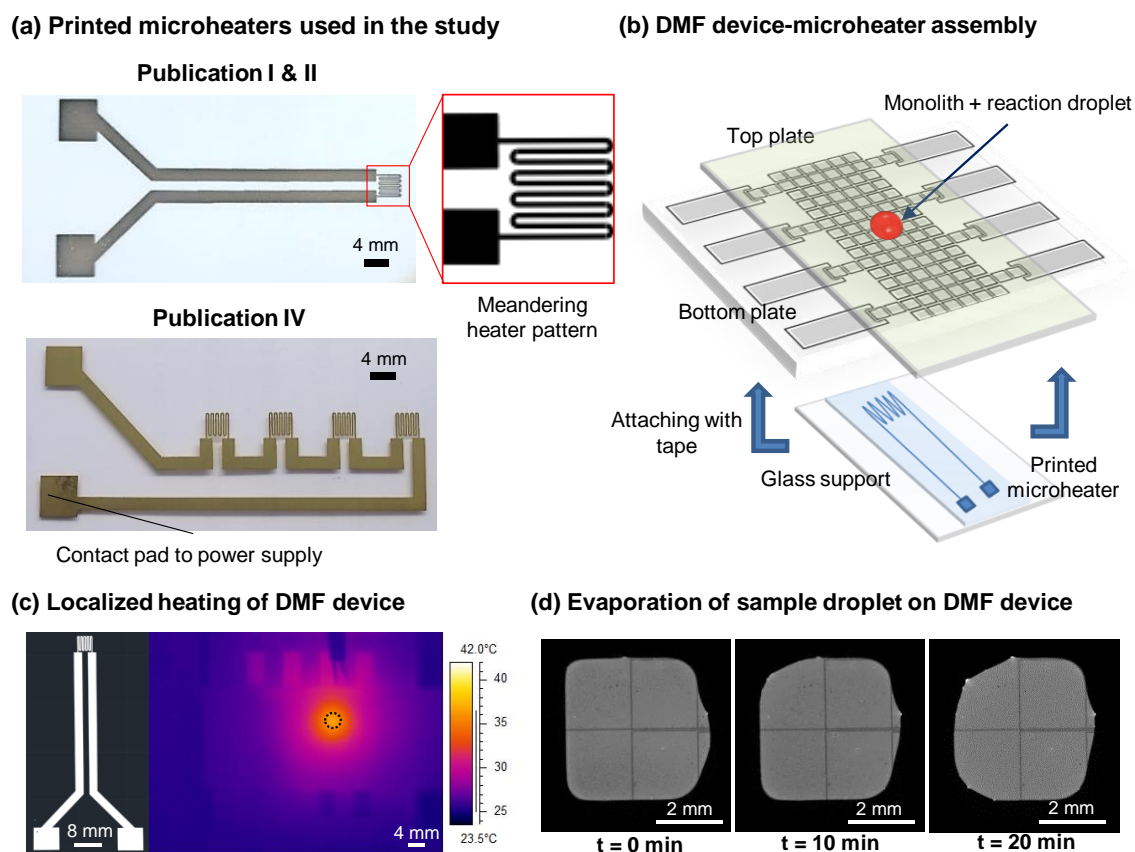


**Figure 9** (a) Inkjet-printed microheaters used in this study: Top-view photographs; Insert: Magnified CAD layout of meandering heater part. (b) Illustration of DMF device-microheater assembly. (c, d) Microheater characterization with four-electrode-sized water droplet (volume ca.  $3\text{ }\mu\text{L}$ ) at a heating power of  $0.1\text{ W}$ : (c) Infrared (IR) thermograph illustrating the temperature distribution on the DMF chip surface (on top-plate) when heated with microheater (circled, area ca.  $4 \times 4\text{ mm}^2$ ), and (d) Fluorescent images illustrating the volume loss of a sample droplet due to evaporation upon heating to  $37\text{ }^{\circ}\text{C}$  at  $t = 0, 10$ , and  $20\text{ min}$ . b–d are modified and reprinted from ref. [114], © 2018 by Sathyanarayanan et al.; Springer nature, CC BY 4.0.

The microheaters were calibrated by inserting a miniature thermocouple from the side of the DMF device into a water droplet ( $\sim 3\text{ }\mu\text{L}$  = volume covering four actuation electrodes) and measuring the temperature of the droplet with the help of a multimeter. In such a way, the temperature difference ( $\Delta T$ ) w.r.t. RT was recorded at constant heating power of  $0.05$ ,

0.1, and 0.15 W. To quantify the loss of a sample volume in a DMF device due to evaporation, micrographs of a water droplet containing rhodamine B dye were captured at every 1 min interval (Figure 9d) and the area of the droplets were calculated using ImageJ and plotted against time to determine the percentage volume loss over time.

### 4.3 Enzyme immobilization

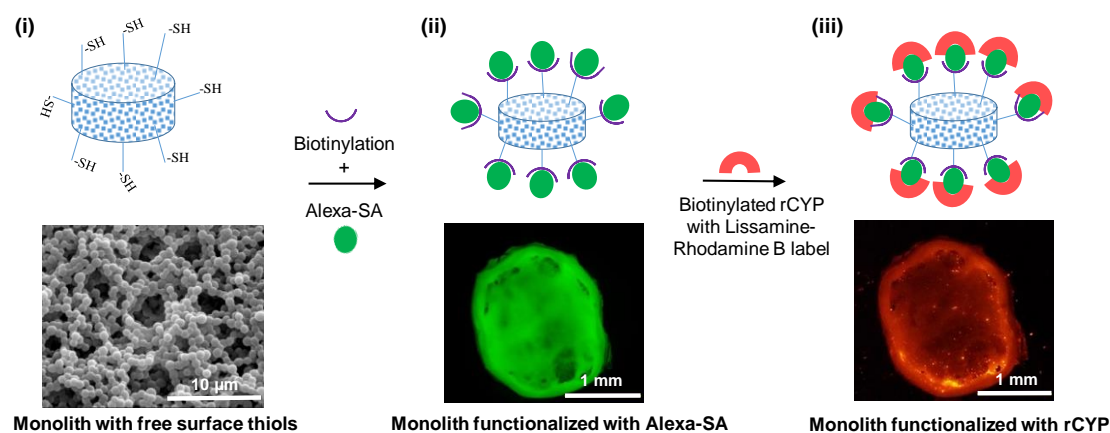
To produce detectable amounts of metabolites, sufficiently high amount of enzymes are needed in the metabolism assays. To immobilize such high amounts of CYP enzymes on a DMF device, two strategies were used in this study: immobilization of (i) rCYP enzymes on porous polymer monoliths in Publications I and II, and (ii) donor HLMs on streptavidin coated magnetic beads in Publication IV.

#### ***Immobilization of recombinant enzymes on porous polymer monoliths***

Porous polymer monoliths bearing excess thiol groups on the surface were fabricated onto the DMF bottom plate by UV curing and functionalizing the monoliths via biotin-avidin chemistry *in situ*. The monolith was fabricated out of thiol-ene (50 mol% excess thiol) by stirring the monomers along with 0.1% (*m/v*) photoinitiator and methanol as porogen following a previously described protocol.<sup>[115]</sup> The emulsion (2  $\mu$ L) was then poured onto the hydrophilic spot (diameter = 2 mm) defined on the bottom plate, then the top plate attached, and cured with UV (1.5 min). As the methanol evaporated quickly during the UV curing, there was no need of an extra step to release the porogens. After curing, the monoliths were thoroughly washed with methanol and let dry. Uniform porosity was obtained with uniformly packed beads with a diameter of 0.5–1.0  $\mu$ m (Figure 10a). The monolith was then sequentially functionalized with biotin and green fluorescent streptavidin, as described in [92] and with the biotinylated recombinant CYP superosomes that also incorporated a red fluorescent stain (Liss-Rhod PE) (Figure 10a). First, the monoliths were biotinylated with 2  $\mu$ L of 1 mM biotin-PEG4-alkyne, cross-linked with 1% (*v/v*) photoinitiator under UV for 1 min. After washing the monoliths with methanol and PBS thoroughly, the excess solvent was allowed to dry before incubating with 2  $\mu$ L of 0.5 mg/mL streptavidin (Alexa-SA) at RT for 15 min. After incubation, monoliths were washed (PBS), followed by incubating with 5  $\mu$ L of rCYP1A1 (Publication I) or 1A2 (Publication II) superosome mixture at RT for 15 min. During incubations, small volumes of PBS were pipetted intermittently to avoid drying. After functionalization, the monoliths were washed with- and stored in PBS until further use.



**(a) Monolith-based CYP immobilization (Publication I and II)**



**(b) Magnetic bead-based CYP immobilization (Publication IV)**

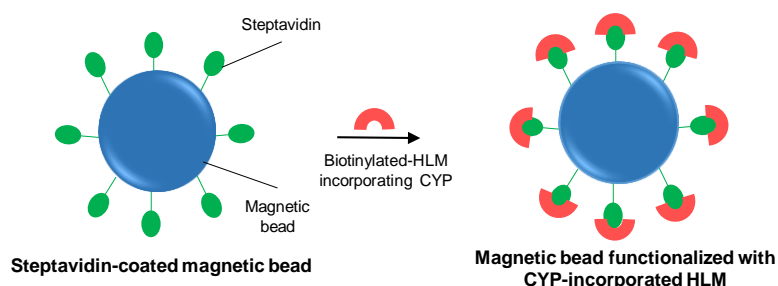


**Figure 10** Schematic illustration of the CYP immobilization process via (a) Functionalization of porous polymer monolith: (i) SEM image of a thiol-ene monolith; and fluorescent images of the monolith functionalized with (ii) Alexa-SA and (iii) rCYP. Revised and reprinted from ref. [114], © 2018 by Sathyanarayanan et al.; Springer Nature, CC BY 4.0 and (b) Functionalization of streptavidin-coated magnetic beads (Dynabeads®) with biotinylated-HLMs of donor samples.

### Immobilization of human liver microsomes on magnetic beads

Microbeads are most commonly used in DMF for heterogeneous immunoprecipitation assays.<sup>[116]</sup> In Publication IV, streptavidin coated magnetic beads (Dynabeads®) were functionalized with biotinylated HLM (Figure 10b). The biotinylated HLM (preparation in Section 3.2) were applied on dry magnetic beads and incubated at RT for 30 min in a rotating mixer. After bead functionalization, the supernatant was removed by holding the beads with the help of magnets. Thereafter, the beads were washed with PBS 3–4 times and then stored in PBS in the refridgerator until further use.

## 4.4 Drug metabolism and drug distribution assays

The activity of the rCYP1A immobilized on monoliths was determined via two assays: (i) fluorescence analysis of Ethoxyresorufin-O-deethylase (EROD) assay to assess rCYP1A1 activity in Publication I, and (ii) mass spectrometric analysis of the metabolite (paracetamol)



produced by phenacetin-O-deethylation via rCYP1A2 in Publication II (Figure 11a). The metabolic clearance capacity (via CYP1A1) of the donor HLMs immobilized on magnetic beads was assessed based on their EROD activity in Publication IV (Figure 11b). Besides enzyme assays, on-chip drug distribution assays that consisted of three-phase liquid-liquid extraction (LLE) of selected pharmaceuticals were carried out in Publication II. The DMF assay protocols are given in the sections below, while the details of buffers, substrates, and metabolite detection wavelengths of drug metabolism assays are given in Table 5.

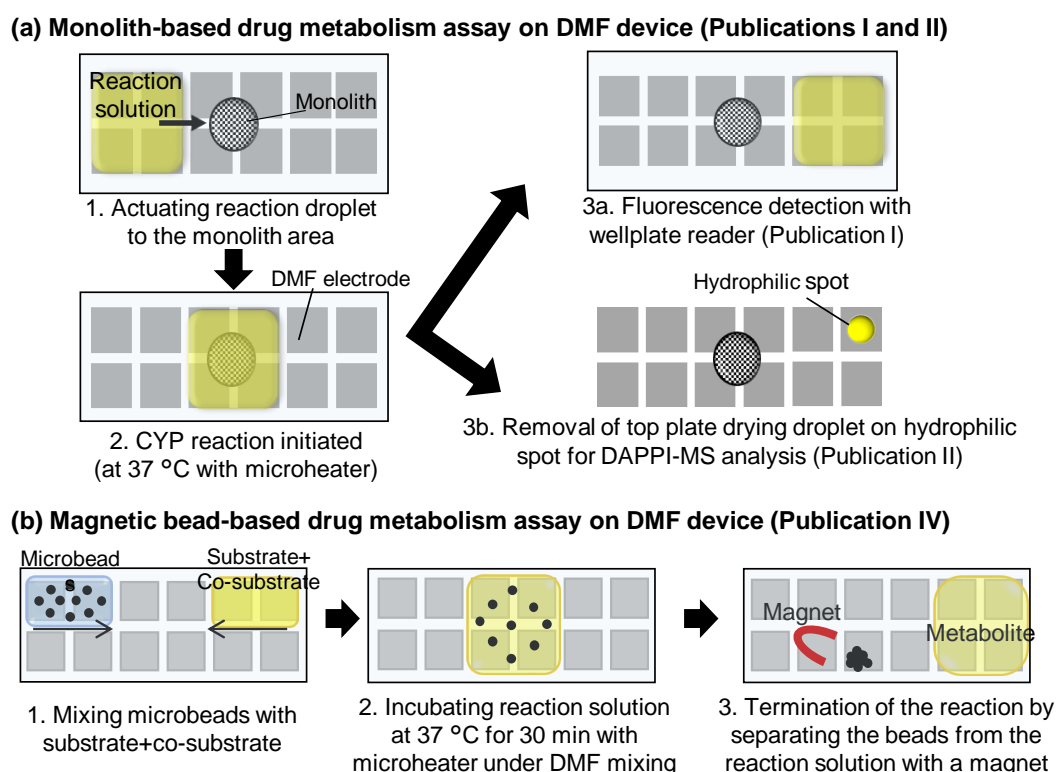


**Figure 11** Schematic illustration of the protocol of on-chip CYP enzyme assays: Determination of activity of (a) rCYP enzymes immobilized on monoliths in Publication I and II, and (b) donor HLMs immobilized on magnetic beads in Publication IV.

### On-chip drug metabolism assays

The rCYP1A assays with monolith-based IMERs (Publications I and II) were carried out with  $\sim 3 \mu\text{L}$  of reaction solution containing substrate and cosubstrate dissolved in buffer containing 0.1% (*m/v*) Pluronic F-68 (reagent details in Table 5). The assays were initiated by bringing the reaction droplet to the monolith incorporating the enzymes and incubating at  $\sim 37^\circ\text{C}$  for 30 min while applying 0.1 W to the microheater (Figure 11a). To compensate the volume loss during incubation (Figure 9d), buffer droplets in size equal to 2 electrodes ( $\sim 1.6 \mu\text{L}$ ) were added to the reaction solution. Incubation was terminated by stopping the heating and bringing the droplet away from the monolith area for further analysis. The fluorescence of the reaction solution originating from resorufin (metabolite) was monitored at ex/em wavelengths of 570/590 nm with a wellplate reader in Publication I, as detailed in

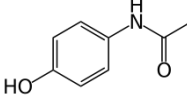
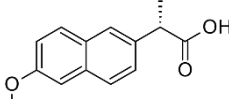
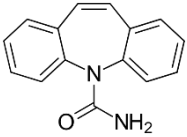
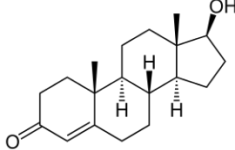
Section 4.5 under “Fluorescence Detection.” In the case of Publication II, the reaction solution was transferred away from the monolith onto a hydrophilic spot and let dry. The dried sample spot was analyzed with ambient mass spectrometry (Details in Section 4.5 under “Mass Spectrometry Detection”).

The bead-based HLM assays in Publication IV were carried out with four parallel reaction solutions, each of ~3  $\mu$ L droplet volume containing substrate, cosubstrate, and HLM incorporated magnetic beads (~1 million) dispersed in a buffer containing 0.1% Pluronic F-68 (reagent concentrations in Table 5). The reaction was initiated by applying 0.2 W to a microheater to incubate the four reaction solutions in parallel at 37 °C for 30 min. The volume loss of the reaction solution due to evaporation was compensated, as mentioned above. The reaction was terminated by stopping the heating and separating the beads from the reaction solution with a magnet (Figure 11b). After reaction termination, the fluorescence of the reaction droplet was monitored at resorufin ex/em wavelengths.

### On-chip drug distribution assays

The feasibility of on-chip LLE for examination of water-octanol distribution of three pharmaceuticals (Table 7), along with the internal standard (testosterone) was determined using two-step extraction schemes, first from the acidic aqueous phase (0.1% TFA, pH 2, acidic functional groups in neutral form) to the organic phase (octanol) and then from the organic phase back to the aqueous phase (ammonium hydroxide, pH 12, acidic functional groups in ionized form) (Figure 12). These extractions were performed by keeping the organic phase (octanol droplet) stationary, while the aqueous droplet was brought in and out of it. After the extraction, the aqueous droplet was transferred onto a hydrophilic spot and let dry. The dried spot was then analyzed with ambient mass spectrometry.

**Table 7** *The chemical structures, monoisotopic masses and chemical properties of the model pharmaceuticals used in Publication II. Molecular properties from Chemicalize (<https://chemicalize.com/>) developed by ChemAxon Ltd. (Budapest, Hungary). Reprinted from ref. [117], © 2018, Sathyanarayanan et al.; MDPI, CC-BY 4.0.*

Compounds	Paracetamol	Naproxen	Carbamazepine	Testosterone
				
Molecular formula	C <sub>8</sub> H <sub>9</sub> NO <sub>2</sub>	C <sub>14</sub> H <sub>14</sub> O <sub>3</sub>	C <sub>15</sub> H <sub>12</sub> N <sub>2</sub> O	C <sub>19</sub> H <sub>28</sub> O <sub>2</sub>
Observed ion type	152.071 ([M+H] <sup>+</sup> )	230.095 (M <sup>++</sup> )	237.102 ([M+H] <sup>+</sup> )	289.216 ([M+H] <sup>+</sup> )
Monoisotopic mass (g/mol)	151.063	230.094	236.095	288.209
pK <sub>a</sub> (acidic)	9.46	4.19	15.96	n.d. (internal qualifier)
LogD (pH 2)	0.9	2.98	2.76	
LogD (pH 12)	-1.15	-0.54	2.76	

([M+H]<sup>+</sup>)=protonated ion, (M<sup>++</sup>)=radical cation and n.d.=not determined

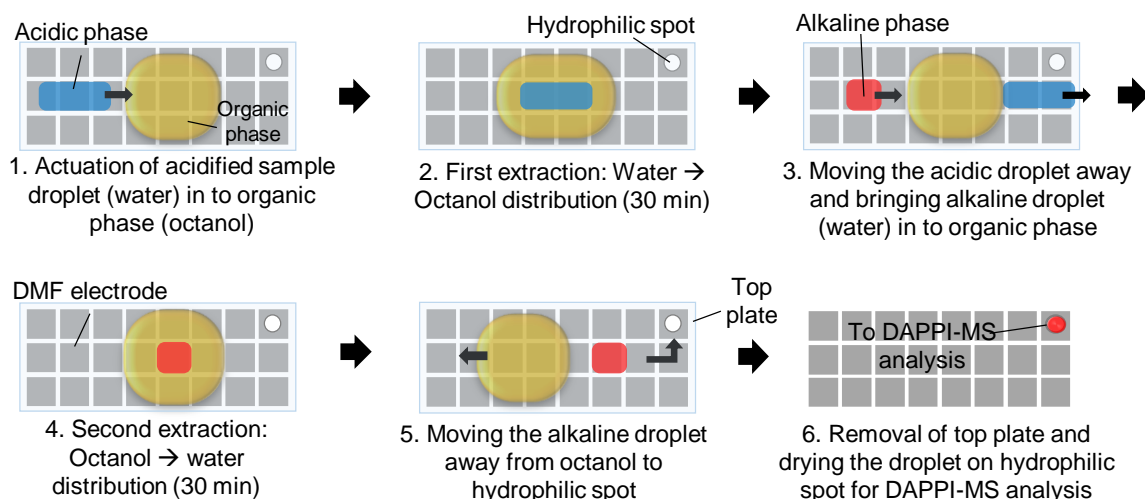


**Figure 12** Schematic view of the steps of on-chip drug distribution assay. Revised and reprinted from ref. [117], © 2018 by Sathyanarayanan et al.; MDPI, CC BY 4.0.

## 4.5 Analytical method interfaces

### Fluorescence detection

For the detection of metabolites produced in on-chip CYP assays in Publications I and IV, the DMF devices were interfaced with a wellplate reader, as described in the reference.<sup>[118]</sup> Interfacing with a wellplate reader makes DMF assays compatible with regular laboratory instrumentation without the need for custom optical setups. The DMF device was taped on top of a well plate lid (96-well) with the analyte droplet(s) aligned along the well(s). The lid was then turned and flipped so that the top plate was facing down before placing the chip on the wellplate reader tray (Figure 13). Thereafter, the fluorescence was measured with the bottom optics of the reader in multi-point mode.<sup>[118]</sup> However, the fluorescence visualization of the functionalized monoliths based on Alexa-SA and lissamine rhodamine B-labelled rCYPs in Publication I (Figure 10a) was performed with a regular epifluorescent microscope.

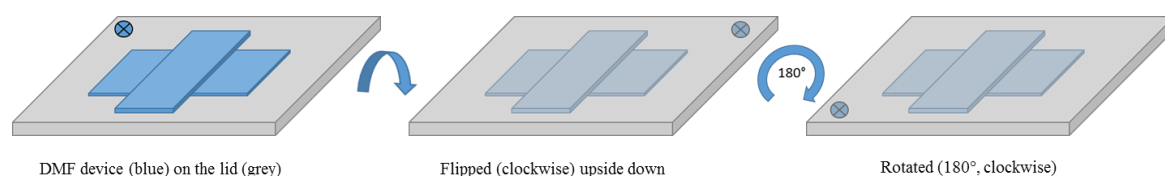


**Figure 13** Schematic representation of the flip and rotation of the DMF device taped on a 96-wellplate lid before placing it inside the plate reader tray. Reprinted from the ref. [114], © 2018 by Sathyanarayanan et al.; Springer Nature, CC BY 4.0.

### **Mass spectrometry detection**

In this study, DMF was interfaced with ambient MS via desorption atmospheric pressure photoionization (DAPPI)<sup>[119]</sup> for the first time. DAPPI is an ambient ionization technique, where the dried samples are desorbed with a heated solvent jet and ionized with UV. The samples from the drug distribution and metabolism assays in Publication II were transferred to the hydrophilic spots on SU-8 dielectric after the reaction. Thereafter, the top-plate was removed and the samples were let dry. The hydrophilic spots were made by covering the SU-8 with circular dicing tapes (diameter = 1 mm) prior to fluoropolymer coating, while the tapes were carefully removed after the baking step (Figure 14a). The dried sample spots were then desorbed/ionized from the DMF bottom plate with the DAPPI system and analyzed with MS (Figure 14b and c), as described in Publication II. Briefly, the sample spots were hit with a jet of chlorobenzene vaporized using a heated nebulizer chip<sup>[120]</sup> (250 °C, 10  $\mu$ L/min) and introduced along with nitrogen (180  $\mu$ L/min) as a nebulizer gas. The UV lamp was fixed ~10 mm above the sample spot to ionize the desorbed sample molecules. The nebulizer chip was fixed at 45° angle w.r.t. DMF plate, while the sample spots were kept at ~2 mm from the MS inlet (Figure 14b and c). For spot-to-spot analysis, the DMF bottom plate was moved with the help of a xyz positioning stage to align the sample spots w.r.t. nebulizer jet and MS inlet (Figure 14d). The extracted ion chromatograms (EIC) were taken with an extraction window of  $\pm 0.05$   $m/z$  and the signal quantitated by integrating the peak area (Figure 14e).

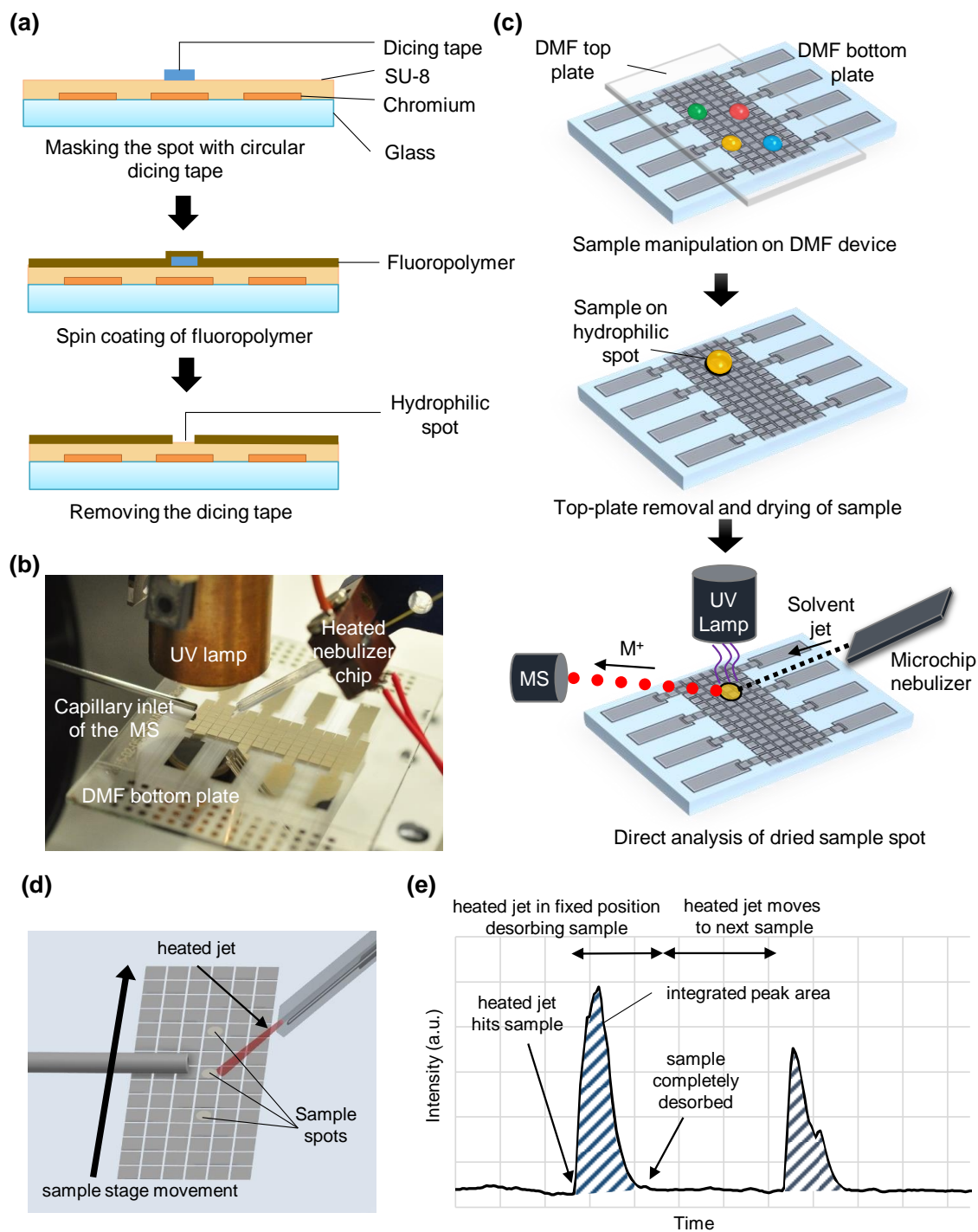


**Figure 14** (a) Schematic view of the fabrication process of digital microfluidic (DMF) bottom plate incorporating hydrophilic spots. (b) Photograph of DMF-DAPPI-MS interface. Schematic illustration of (c) the process flow of DMF-DAPPI-MS analysis, (d) the process of desorption/ionization of samples from the DMF chip surface, and (e) integration of the peak area of extracted ion chromatogram (EIC) in DAPPI-MS analysis. Modified and reprinted from ref. [117], © 2018 by Sathyanarayanan et al.; MDPI, CC BY 4.0.

## DMF-to-microchannel interface

In Publication III, OSTE was used for implementation of DMF-to-channel microfluidic interface. A custom interface for sample delivery from DMF part to the microchannel part was developed and a thiol-ene based microchip electrophoresis unit was modularly integrated with the DMF bottom plate featuring thiol-ene dielectric. The bonding quality was confirmed with an electrophoretic injection and a subsequent fluorescence detection of 5  $\mu$ M Oregon green dye. The channel was filled with a borate buffer containing 0.1% (*m/v*) SDS prior to the injection of the sample. For this purpose, the DMF chip, along with the pogo pin connector of the DropBot controller, was placed on the microscope sample stage (Figure 15a). The sample was loaded with an electric field of 400 V/cm applied over the injection channel (20 s) and injected by applying electric fields of 750 V/cm over the separation channel. Push back voltages were then applied to the injection inlet and outlet (Figure 15b). The fluorescence of the injected Oregon green sample plug was monitored perpendicular to the microchannel at the effective separation length of 33 mm and recorded with a photomultiplier attached to the microscope and an AD converter. The droplet transfer at the digital-to-channel microfluidic interface was visualized with a water droplet containing food color in Figure 15c.

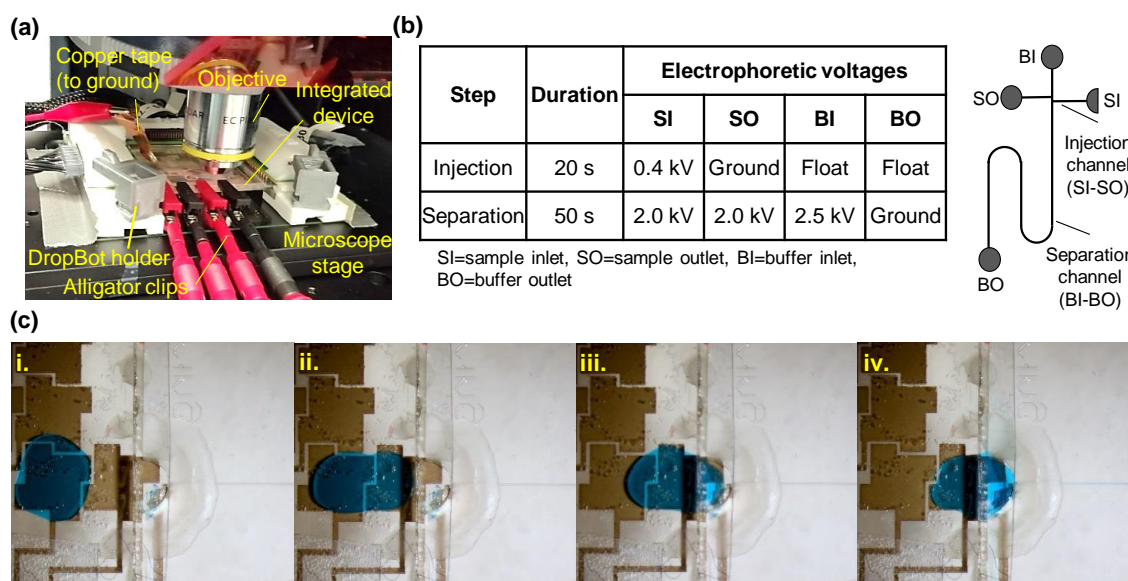


**Figure 15** (a) Photograph of DMF-electrophoresis set up under the microscope. (b) Tabular presentation of electrophoretic voltages used for the injection of 5  $\mu$ M Oregon green fluorescent dye along with the schematics of the microchannel. (c) Still photographs of a blue food color droplet (in water) transferred from the DMF part to the microchannel part: (i-ii) Actuation of the droplet with DMF towards the microchannel inlet; (iii) Filling of the microchannel inlet; and (iv) Filling of the microchannel as soon as the inlet is filled. Modified and reprinted from ref. [121], © 2020 by Sathyanarayanan et al.; WILEY-VCH Verlag GmbH & Co. KGaA, Weinheim, CC BY 4.0.

## 5 Results and discussion

### 5.1 Selection of dielectric material

In this study, SU-8 (Publications I and II) and thiol-enes (Publications III and IV) were selected as the primary dielectric materials based on their: (i) positive dielectric properties for prolonged DMF actuation; (ii) low optical background in Publications I and IV; (iii) good thermal stability on DAPPI in Publication II; and (iv) compatibility towards bonding/integration and low non-specific interactions in Publication III.

Parylene C is a widely used dielectric material in DMF because it allows for defect-free coating by chemical vapor deposition (CVD). However, CVD is a process that requires expensive instrumentation.<sup>[122]</sup> Therefore, spin-coatable polymers, such as SU-8, have been used as an alternative dielectric material in DMF applications. SU-8 also enables patterning by photolithography for complex fluidic integration (if needed) and has a high dielectric constant of 3.5.<sup>[123]</sup> Thus, SU-8 was chosen as the dielectric layer in this study. Thiol-enes, a class of polymers introduced to microfabrication in recent years,<sup>[110]</sup> also possess similar characteristics and advantages as SU-8, and has a dielectric constant of 5.1.<sup>[124]</sup> The feasibility of SU-8 for DMF has been established in the previous literature, whereas thiol-enes were introduced to DMF as a dielectric for the first time in this study. In this section, feasibility of SU-8 and thiol-enes for DMF will be discussed and compared with the view to: (i) dielectric properties, (ii) *in situ* optical detection, (iii) ambient MS detection, and (iv) integration with microchannel.

When spin-coated on a glass substrate, both SU-8 and thiol-ene polymers yielded a smooth surface. However, when coated on porous Novele substrate (Figure 16a), SU-8 layer was uneven and resulted in a wavy type of surface (Figure 16b). This was likely due to the reflow of SU-8 to the pores of the Novele substrate as a result of solvent evaporation during the SU-8 soft-bake. In contrast, the solvent-free thiol-ene does not suffer from reflow. As a result, smooth planar surfaces were obtained with thiol-ene on Novele substrate (Figure 16c) and therefore, it was chosen as dielectric for inkjet-printed devices in Publication III. The dielectric performance of both SU-8 and thiol-ene coated devices were comparable to those of Parylene C coated devices with typical actuation voltages of 80–120 V<sub>rms</sub> at 10 kHz. Under these driving voltages, SU-8 and thiol-ene coated devices could be used for long term (>30 min) continuous actuations for several cycles. The performance of thiol-ene as a dielectric layer was evaluated in Publications III (inkjet-printed devices) and IV (glass-based devices). The droplet velocities on thiol-ene layer under actuation were compared with those on Parylene C (Figure 16d). Irrespective of the monomer composition (allyl-rich, thiol-rich or stoichiometric), the droplets' velocities on thiol-ene were similar to those on Parylene C.



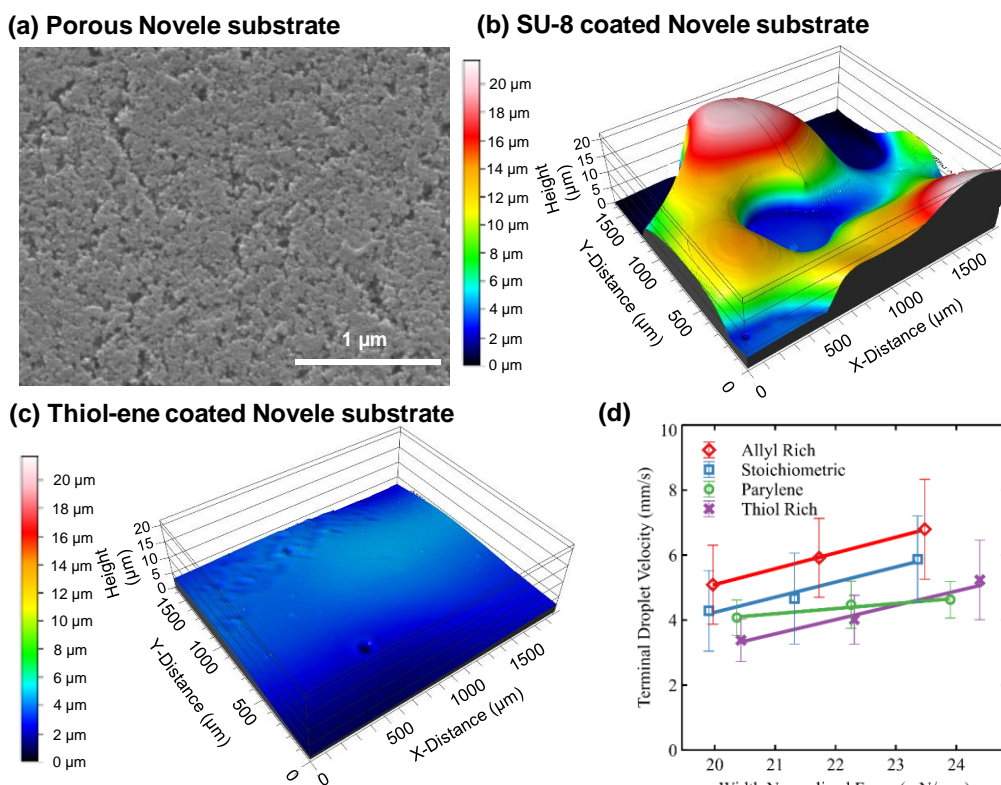


**Figure 16** (a) SEM image of Novele substrate. (b,c) 3D profilometer data of the surface of: (b) SU-8- and (c) Thiol-ene coating on Novele substrate. (d) Force-velocity plot of 1  $\mu$ L droplets (water containing 0.1% Tetricon) actuated on inkjet-printed DMF devices coated with Parylene C and different compositions of thiol-ene. b–d are modified and reprinted from ref. [121], © 2020 by Sathyanarayanan et al.; WILEY-VCH Verlag GmbH & Co. KGaA, Weinheim, CC BY 4.0.

However, one key advantage of thiol-ene as dielectric over SU-8 is its very low autofluorescence in the UV-range (Figure 17). This is particularly important for sensitive detection of the probe CYP metabolites, some of which fluoresce at near-UV wavelengths. Therefore, based on the fluorescence of the CYP probe metabolites used, SU-8 and thiol-ene were used in Publications I and IV, respectively.

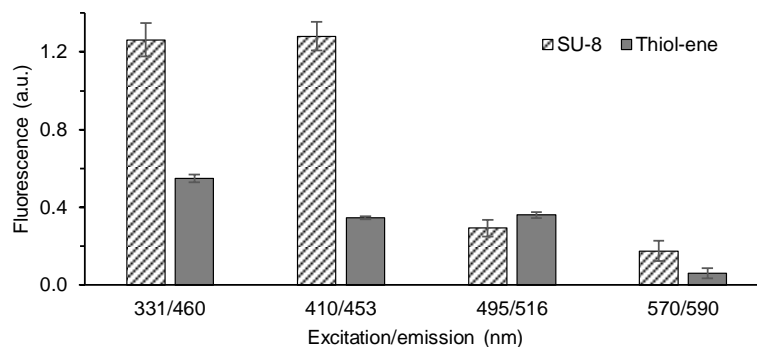


**Figure 17** Fluorescence background of SU-8 and thiol-ene coated DMF devices at different metabolite detection wavelengths (probe metabolites listed in Table 5).



Concerning ambient MS, the most critical properties of the substrate plate are thermal and solvent stabilities. In DAPPI, a hot ( $>200\text{ }^{\circ}\text{C}$ ) jet of vaporized chlorobenzene is directed at sample spots during desorption/ionization (Figure 14c). Out of the materials tested, thiol-ene has a lower glass transition temperature ( $53 \pm 2\text{ }^{\circ}\text{C}$ )<sup>[125]</sup> than that of SU-8 ( $240\text{ }^{\circ}\text{C}$ ).<sup>[126]</sup> Although both polymers show good solvent stability, thiol-ene would not have tolerated such a high temperature jet of organic solvent vapor. Therefore, SU-8, which was stable under harsh conditions due to its high thermal stability and high degree of cross linking, was chosen as the dielectric material for DAPPI-MS analysis in Publication II. No visual damage was observed on the SU-8 surface after the normal desorption time of 1–2 minutes. This was also evident from the MS spectra, which showed no background ion interference from SU-8 (Figure 18a).

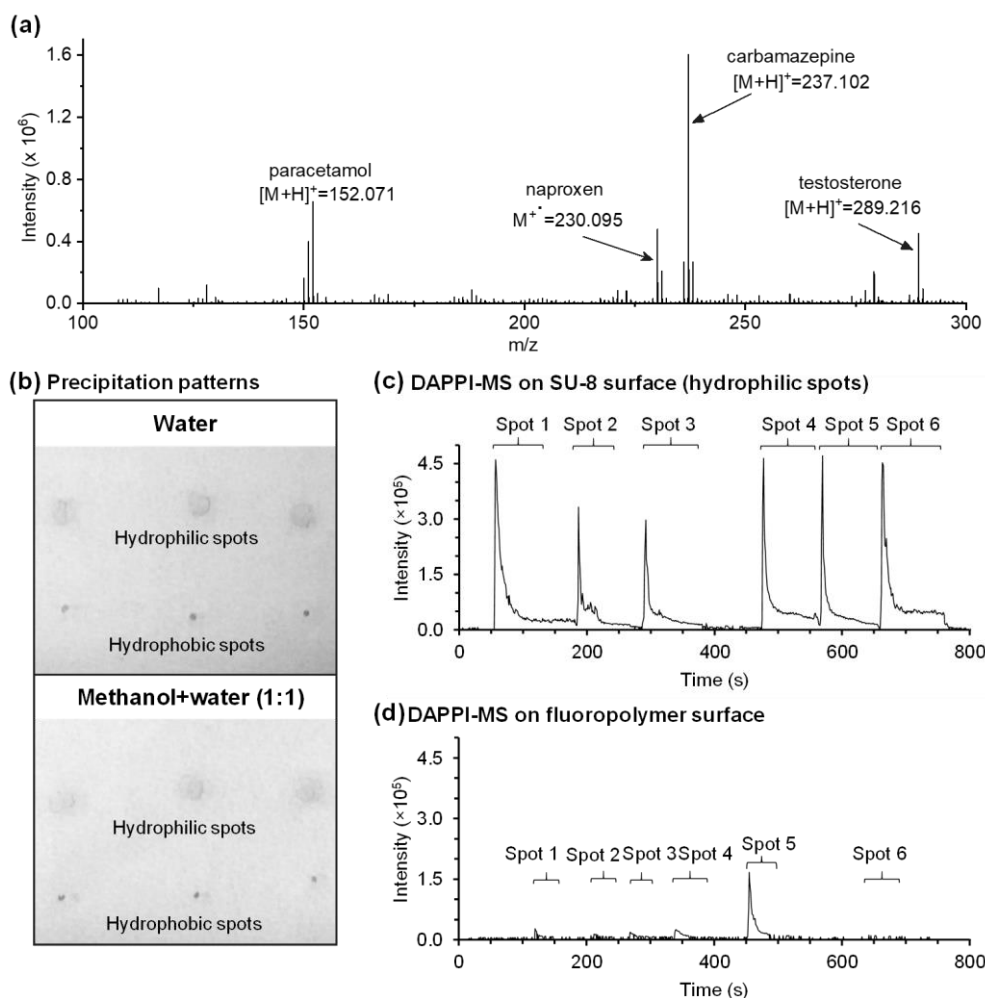


**Figure 18** (a) Mass spectrum of paracetamol (66 pmol), naproxen (44 pmol), carbamazepine (42 pmol), and testosterone (70 pmol) dissolved in methanol-water (1:1), deposited onto the hydrophilic SU-8 spot, and analyzed by DAPPI-MS. (b) Photograph of rhodamine B precipitation pattern on hydrophilic SU-8 spots and on hydrophobic fluoropolymer in water and methanol-water. (c,d) EICs of testosterone (internal qualifier, 70 pmol in methanol-water) deposited and analyzed from parallel spots ( $n = 6$ ) by DAPPI-MS: (c) on hydrophobic fluoropolymer, and (d) on hydrophilic SU-8 spots. Modified and reprinted from ref. [117], © 2018 by Sathyanarayanan et al.; MDPI, CC BY 4.0

The efficiency of the desorption process in DAPPI highly depends on the uniformity of the sample precipitation pattern, which is largely impacted by the wetting properties of the surface.<sup>[127]</sup> The fluoropolymer surface resulted in tiny, dense precipitation (Figure 18b), which was difficult to target with the heated solvent jet and thus, resulted in poor repeatability (Figure 18c). Instead, drying the sample (dissolved in aqueous solvent) on SU-8 spots resulted in a uniformly spread precipitation pattern (Figure 18b), which substantially improved scan-to-scan repeatability (Figure 18d). Additionally, the hydrophilic SU-8 spots also helped anchor the sample droplets to the bottom plate while removing the top plate for the sample to evaporate prior to DAPPI-MS analysis.

In principle, both SU-8 and thiol-enes enables the integration of multiple, bonded layers via lithographic processing + adhesive bonding and replica molding + bonding, respectively. In the case of SU-8, the microchannel layer would have to be spin-coated on top of the dielectric layer and adhesively bonded using mask aligner.<sup>[128]</sup> However, thiol-enes allowed us to replicate the channel separately and to bond on demand onto the bottom plate, which is a less-complicated process, especially with respect to creating sealed microchannels.<sup>[109]</sup> Thus, thiol-ene-on-thiol-ene bonding was used to integrate a microchannel on the DMF platform in Publication III. The microchannel integration is elaborated in detail in the next section.

## 5.2 Digital-to-channel microfluidic interface

The integration of the DMF platform with microchannel networks was examined in this study with a view to carry out sequential fluidic operations on analytical lab-on-a-chip platforms. Previous attempts to integrate these two fluidic concepts include, for example, an open DMF platform integrated with a PDMS microchannel,<sup>[48]</sup> a 2-layered micromachined glass device featuring DMF and microchannel parts,<sup>[49]</sup> or two separate DMF and microchannel devices interfaced using a capillary.<sup>[50]</sup> In this study, these two systems were integrated on a single substrate/platform, where both droplet actuation and channel fluidic operations take place. This was accomplished by: (i) inkjet printing the DMF electrodes on flexible substrate; (ii) spin-coating the substrate with thiol-ene dielectric and partially with fluoropolymer; and (iii) fabricating and bonding a thiol-ene microchannel onto the thiol-ene coated substrate free from fluoropolymer (Figure 19a). As discussed in the previous chapter, the inkjet printing of DMF electrodes and the spin-coating of thiol-ene dielectric allows for rapid prototyping and the low-cost manufacturing of devices without compromising DMF performance. The thiol-ene microchannel can be fabricated by cleanroom-free replica molding<sup>[109]</sup> and bonded to the thiol-ene coated bottom plate free from fluoropolymer. In this study, inkjet-printed electrodes also served as MCE electrodes thanks to the ability to pattern thiol-ene by masked photolithography to expose the MCE electrodes. The thiol-ene microchannel was bonded onto the DMF substrate carefully in a way that the electrode feeding the droplet was partially inside the sample inlet of the microchannel (Figure 19b). The bonding quality of the thiol-ene microchannel was confirmed by electrophoretic injection and the subsequent fluorescence detection of Oregon green dye. The electrophoresis performance (peak shape) is very sensitive to any leakage

and thus, is a good indicator of defects in the microchannel bonding quality. Figure 19c shows the signals from four consecutive injections of Oregon green. The narrow and symmetric peaks (peak width at half-height of 1.2 s) and good migration time repeatability (3.8% RSD) are evidence that the bonding quality was good.

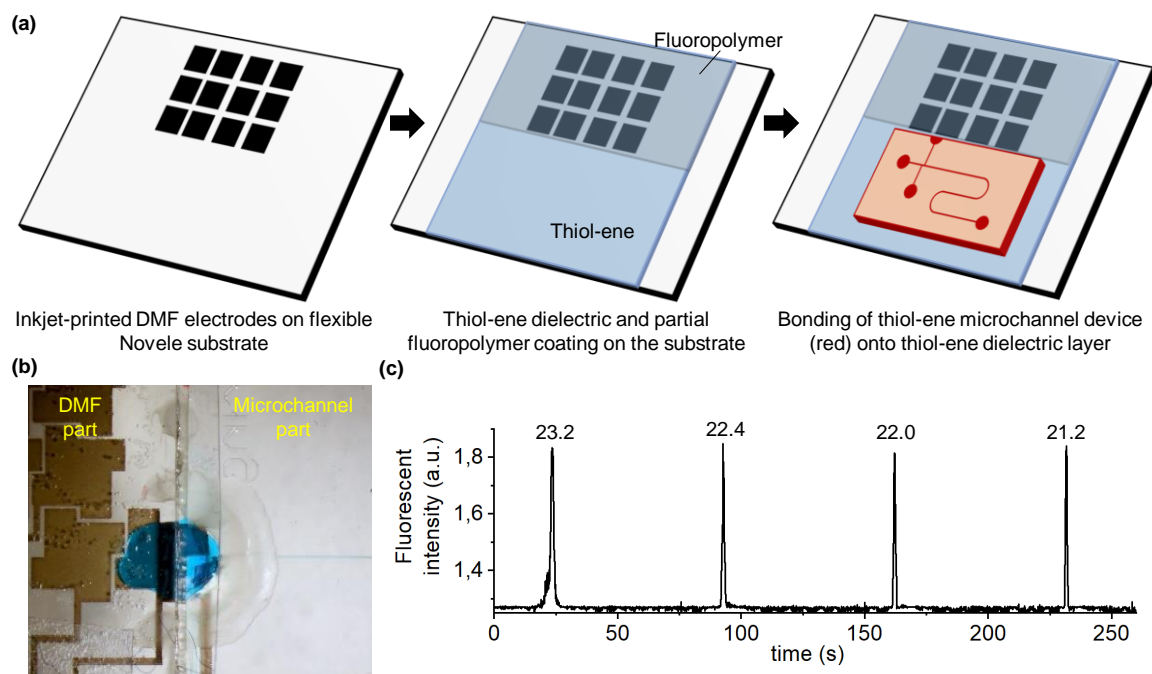


**Figure 19** (a) Schematics of steps involved in the fabrication of integrated DMF-microchannel device. (b) Photograph of droplet transfer (food colorant in water) from the DMF part to the microchannel inlet and subsequent filling of the microchannel. (c) Fluorescent signal (PMT voltage) from  $n = 4$  consecutive injections of  $5 \mu\text{M}$  Oregon green dye with migration times on top of the peaks (from injection cross to the point of detection). c is modified and reprinted from ref. [121], © 2020 by Sathyanarayanan et al.; WILEY-VCH Verlag GmbH & Co. KGaA, Weinheim, CC BY 4.0.

The bench-top, cleanroom-free approaches used in this DMF-microchannel interface, such as the inkjet printing of electrodes, UV patterning of thiol-ene dielectric and microchannel layer, as well as the bonding of the microchannel layer, significantly reduces the cost. The cost of materials of fully integrated DMF-microchannel device with- and without supporting structures (adhesive tapes and support glass plates) are \$1.34 and \$0.74 (USD), respectively (detailed cost breakdown can be found in publication IV). Also, these approaches can potentially be scaled up to high-volume manufacturing via roll-to-roll printing and coating,<sup>[35]</sup> and roll-to-plate imprinting and sealing.<sup>[129]</sup>

## 5.3 Development of droplet-scale CYP reactors

### 5.3.1 Heating of CYP reactors and evaporation effects

Most of the DMF-based assays reported in the literature use DMF for only short-term operations at RT. However, in this study, the enzyme reactions require elevated temperatures and relatively longer incubation times; thus, the longevity of the devices (as demonstrated in Chapter 5.1) and evaporation is an issue. Hence, the heating and cooling curves, as well as the sample evaporation, were carefully studied in this study. Irrespective of the heating power, the temperature of the droplet increases rapidly upon heating for the first two minutes and then reaches the plateau at about 10 minutes (Figure 20a). This was also true in the case of both single heaters (Publications I and II) and multiple heater patterns (Publication IV) (Figure 9a). In Publication IV, four droplets could be evenly and locally heated in parallel (Figure 20b). This localized heating is critical in preventing the degradation of NADPH (crucial cofactor of CYP reactions) before the reaction. Even though the devices used in the study are in a 2-plate DMF configuration, the loss of solvent due to evaporation from the gap between the top- and bottom plate is inevitable. CYP enzyme reactions are usually carried at the physiological temperature for several minutes<sup>[130]</sup> and thus, evaporation becomes significant in these assays. The volume loss after 10 minutes was found to be about 5% at RT and about 12.5% at 37 °C (Figure 20c). As such, the volume loss over time was linear (while heating), while the compensating volume of the buffer to be added could be somewhat precisely extrapolated based on the evaporation curve (Figure 20c).

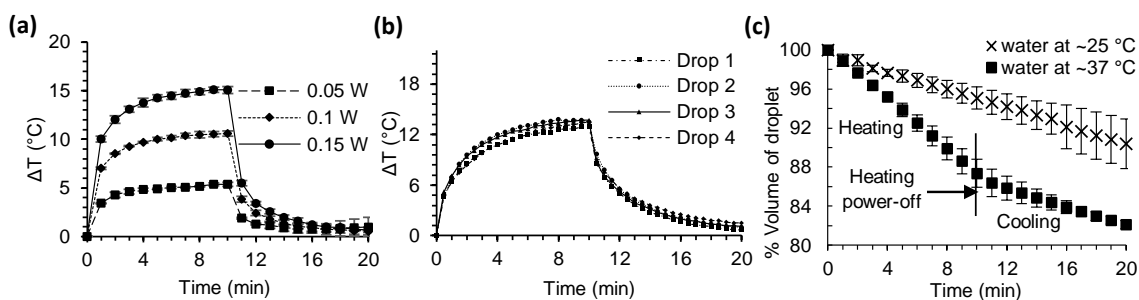


**Figure 20** Microheater characterization with sample droplet of four actuation electrodes (volume ca. 3  $\mu$ L): (a, b) Thermal stabilization curves for the heating and cooling cycles obtained from single meander microheater at different heating powers (a), and four parallel droplets heated with four microheaters at 0.2 W of total heating power (b). (c) Effect of heating and cooling back to room temperature on the volume loss of the sample in comparison to the constant decrease in volume at RT. The error bars represent the deviation between  $n = 5$  parallel microheaters in a and  $n = 3$  repeated experiments in c. a and c were adjusted and reprinted from ref. [114], © 2018 by Sathyanarayanan et al.; Springer Nature, CC BY 4.0.

During DMF assays, appropriate volumes of buffer droplets were added to the reaction solution to compensate for the evaporation and thereby, minimize variation in the

concentration of substrate and cosubstrate during incubation. Unlike previously used heating systems on DMF, such as peltier element,<sup>[80]</sup> metal heating block,<sup>[79]</sup> and lithographically patterned microheaters,<sup>[131,132]</sup> the printed microheaters enable on-demand customization of assay design by simply redesigning and printing new microheater patterns.

### 5.3.2 Selection of enzyme immobilization approaches

The success and homogeneity of rCYP and HLM immobilization on the monoliths and beads could be monitored with the help of the rhodamine tag embedded on the liposomes used for the bioinylation step. The rCYPs bound onto the monoliths were quantified indirectly based on the EROD activity of rCYP1A1 and found to be ca.  $0.9 \pm 0.4$  fmol ( $n = 10$  reactors), assuming that the activity of the immobilized enzymes is similar to that of the soluble rCYP1A1. The resulted larger variation of ~44% in the amount of rCYP1A1 is likely due to the lack of precise control in the surface area of the monoliths, a usual downside of the monolith systems used in microfluidics in general. Therefore, the developed monolith based enzyme reactor is best suited for qualitative metabolic profiling, such as the identification of unknown metabolites by ambient MS, as demonstrated in Publication II. In Publication IV, streptavidin-coated magnetic microbeads were functionalized with HLMs, as the beads could be separated and retrieved after the assay incubation. This gives the bead-based assays more flexibility in terms of device reusability over monolith-based assays, where the monoliths are permanently fixed onto the device and thus, are single-use. In addition, the HLMs have a broad size distribution, ranging from a few-hundreds-of-nanometers to a few-micrometers. Therefore, b-HLMs might clog the monoliths.

The activities of the immobilized rCYPs were determined by using ethoxyresorufin O-dealkylation to resorufin (EROD) via CYP1A1 (Publication I) and that of immobilized HLMs by using EROD; CEC dealkylation to CHC via CYP1A2; coumarin 7-hydroxylation to umbelliferone via CYP2A6; and dibenzylfluorescein dealkylation to fluorescein via CYP3A4 (Publication IV) as the model reactions. In terms of specificity, the CYP1A model reactions did not suffer from the interference from any background signals. In Publication I, resorufin was detected on-chip with sufficiently good sensitivity (LOD = 36 fmol and LOQ = 109 fmol) and linearity ( $R^2 = 0.99$ ; range 0.15–15 pmol) at droplet-scale (Figure 21a). However, substantial fluorescence backgrounds originated from NADPH and substrate at the detection wavelengths of umbelliferone (331/460 nm) and fluorescein (495/516 nm), respectively (Figure 21b). These background signals were considered while determining the metabolite production of CYP2A6 (umbelliferone) and 3A4 (fluorescein). The metabolites were detected on-chip with sufficiently good sensitivity compared to the blanks (signals from substrate and cosubstrate) (Table 8). Based on the background signals, umbelliferone and fluorescein probe reactions would require the separation of components prior to metabolite detection and therefore were not selected as model reactions for further CYP assays on-chip. The effect of the number of functionalized beads on metabolite production on-chip was evaluated with the CEC probe reaction. This is particularly significant because the difference between the signals from the samples cannot be quantified if the system gets saturated. The response (metabolite production rate) was found to be increasing linearly, along with an increasing number of beads (Figure 21c) and thus, the

highest test number of beads (~1 million) was chosen for further on-chip assays. At this concentration, the beads were unlikely to cause much impact on the electrowetting properties of the aqueous sample droplet.<sup>[133]</sup> Since resorufin has a lower on-chip detection limit than CHC (Table 8), the EROD reaction was chosen for the on-chip diagnostic CYP assays for the assessment of metabolic capacity of individual donor samples.

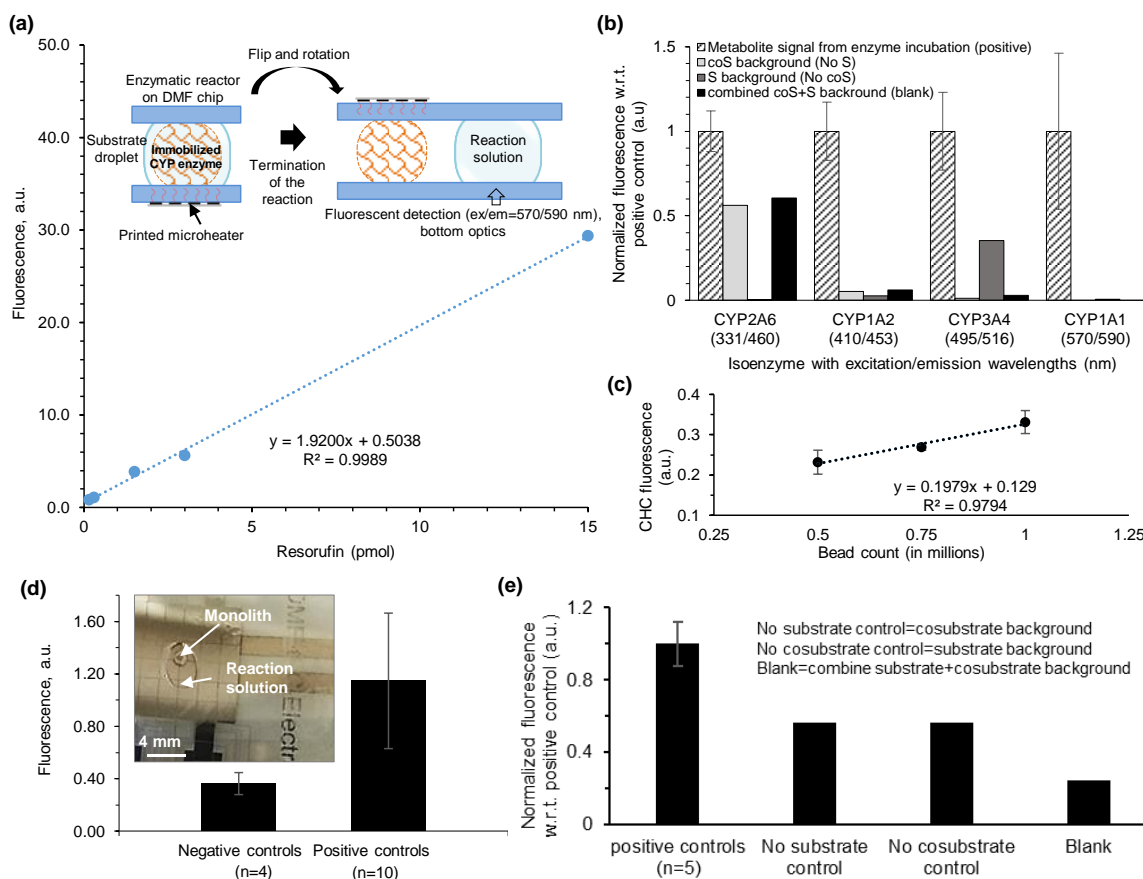


**Figure 21** (a) Resorufin calibration curve and schematics of the fluorescence quantification by well-plate reader. (b) Selectivity of the metabolite quantitation from model probe reactions using immobilized enzymes off-chip; error bars: SD from  $n = 3$  assays for CYP1A1 and  $n = 4$  assays for the rest. (c) Effect of bead count on CHC metabolite production of pooled HLM on-chip; error bars: SD from  $n = 3$  assays. (d) The fluorescence signal of the reaction solutions (positive controls,  $n = 10$ , and negative controls,  $n = 4$ ) extracted from the monolith-based rCYP1A1-reactors. (e) Selectivity of EROD assay form the bead-based HLM-reactors with pooled HLM ( $n = 20$  donors). a and d are modified and reprinted from ref. [114], © 2018 by Sathyanarayanan et al.; Springer Nature, CC BY 4.0.

**Table 8**      *The limits of detection (LOD) of metabolites of selected on-chip probe reactions produced from pooled HLM immobilized on magnetic beads.*

Metabolite <sup>a</sup>	Ex/em (nm)	LOD (pmol)	Linearity (R <sup>2</sup> )
Umbelliferone (CYP2A6)	331/460	1.04	0.992
3-cyanoumbelliferone (CHC) (CYP1A2)	410/453	0.26	0.9878
Fluorescein (CYP3A4)	495/516	0.04	0.9987
Resorufin (CYP1A1)	570/590	0.08	0.9824

<sup>a</sup> Detected in respective buffers containing substrate and cosubstrate (concentrations given in Table 5). Ex/em = excitation and emission wavelengths.

The EROD reactions on-chip were found to be sensitive enough that the fluorescence response of metabolites produced from the assays was higher than those of the control experiments (no substrate, enzymes or heating) and blanks (substrate + cosubstrate in buffer) (Figure 21d and e). The difference between the average signals from the positive and negative controls is statistically significant, as  $p = 0.001$  and  $0.026$  in monolith- and bead-based assays on DMF, respectively. Furthermore, the average resorufin (metabolite) production rates of monoliths functionalized with rCYP1A1 and beads functionalized with HLM were  $20.3 \pm 9.0$  and  $6.8 \pm 1.2$  fmol/min, respectively.

### 5.3.3 Mass spectrometry detection of metabolites

For metabolite identification purposes, interfacing DMF with ambient MS is by far the most straightforward approach; however, it has not been thoroughly examined before this work. The integration of a monolith based CYP reactor with DAPPI-MS could be a potential alternative approach for preliminary metabolic profiling, i.e., identification of the most abundant metabolites of new drug candidates at the early stages of drug discovery. Nevertheless, this approach is not readily feasible for the quantitative determination of clearance rates similar to that of the fluorescence-based approach. This is due to the inherently high variation of signals in DAPPI-MS analysis, which in this study, was 35% and 23% RSD for paracetamol (66 pmol;  $n=5$  spots) on SU-8 and PMMA (a common substrate for DAPPI-MS)<sup>[134]</sup> surfaces, respectively. The lower limits of detection (LLOD) of the pharmaceuticals (listed in Table 7) were calculated from  $n=5$  replicate spots and defined as the lowest concentration at which the analyte gave a detectable signal at all five spots. The LLODs of paracetamol, naproxen, and carbamazepine were 1  $\mu\text{g/mL}$  (7 pmol), 0.25  $\mu\text{g/mL}$  (1 pmol), and 0.5  $\mu\text{g/mL}$  (2 pmol), respectively (tested range: 0.1–10  $\mu\text{g/mL}$  in methanol-water 1:1). Thus, the developed method is most feasible for measuring pharmaceuticals from biological matrices, such as plasma or urine, where the drug concentrations are usually in the range of  $\mu\text{g/mL}$ .

The feasibility of DMF-DAPPI-MS interface for detecting the metabolites of CYP reactions was demonstrated with phenacetin O-deethylation assay using rCYP1A2 immobilized onto the porous polymer monolith. In general, CYP assays are carried out in buffers with relatively high salt content such as Tris or phosphate buffers at physiological

pH (7.4–7.5). The phosphate buffer is non-volatile and leaves a dense precipitate upon evaporation, which makes it inherently unfavorable for any ambient MS analysis. Therefore, more volatile Tris was chosen in this study and the signal intensity of paracetamol in Tris was observed to be similar to that in methanol-water (1:1) solvent (Figure 22a). The metabolite paracetamol produced from the on-chip CYP assays was detected as protonated Tris adduct ion  $[M + \text{Tris} + \text{H}]^+ = 273.199$  (Figure 22b). As seen in Figure 22b, the DMF-DAPPI-MS method is sensitive enough to detect the trace amount of metabolites (few pmol) from the on-chip assays, while no metabolite was detected from the negative control (without substrate).

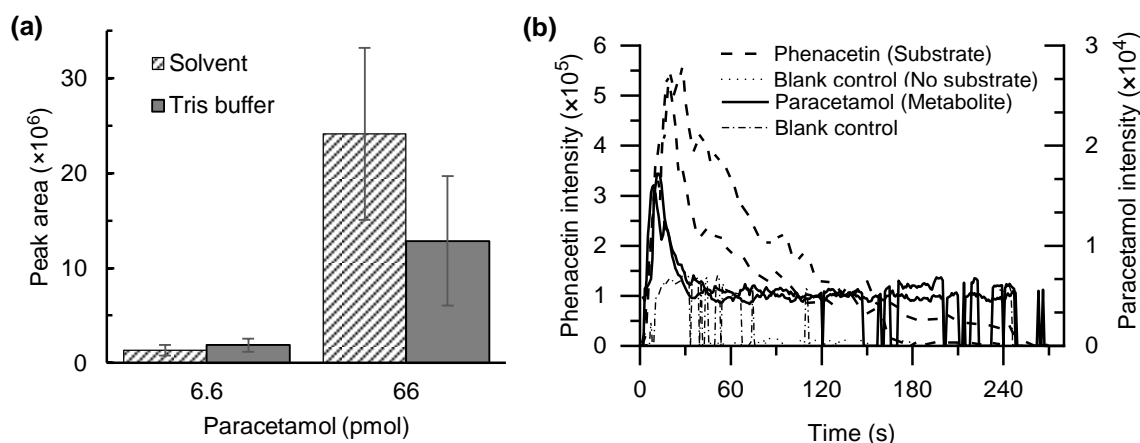


**Figure 22** (a) Comparison of paracetamol signal intensities in pure solvent (methanol-water 1:1) vs. 60 mM Tris buffer ( $n = 5$  samples each). (b) EICs of paracetamol (bold line) produced via CYP1A2 mediated phenacetin (bold dotted line) O-dealkylation analyzed from the dried precipitate of the enzymatic reaction solution after the on-chip drug metabolism assays. Modified and reprinted from ref. [117], © 2018 by Sathyanarayanan et al.; MDPI, CC BY 4.0.

Octanol-water distribution is the usual tool for the assessment of drug solubility and for purification of lipophilic compounds from buffer solutions featuring high salt concentrations. The DMF-based droplet handling enables small volume sample preparation, e.g., liquid-liquid (micro)extraction (LLE), prior to reaction or analysis.<sup>[135]</sup> Therefore, the feasibility of the developed DMF-DAPPI-MS interface was also demonstrated for LLE of selected pharmaceuticals via octanol-water distribution. This was carried out by a three-phase (aqueous→organic→aqueous) liquid-liquid extraction (LLE) of naproxen, paracetamol, and carbamazepine on DMF. The compounds' distribution varied based on their water solubility and acidity (Table 7). Naproxen being the most acidic ( $\text{pK}_a$  4.19), moderately lipophilic ( $\log D$  2.98) at pH 2 and weakly lipophilic ( $\log D$  -0.54) at pH 12, was efficiently extracted from the aqueous to the organic phase in its neutral form and also from the organic to the aqueous phase back in ionized form. Whereas, paracetamol, being more water soluble ( $\log D$  0.91) at pH 2, the extraction from the aqueous to the organic phase was not as efficient as naproxen (Figure 23a). Carbamazepine, being weakly acidic ( $\text{pK}_a$  15.96) with lower water solubility ( $\log D$  2.76), was not back-extracted from the organic to the final aqueous phase, and only paracetamol and naproxen were detected (Figure 23b).



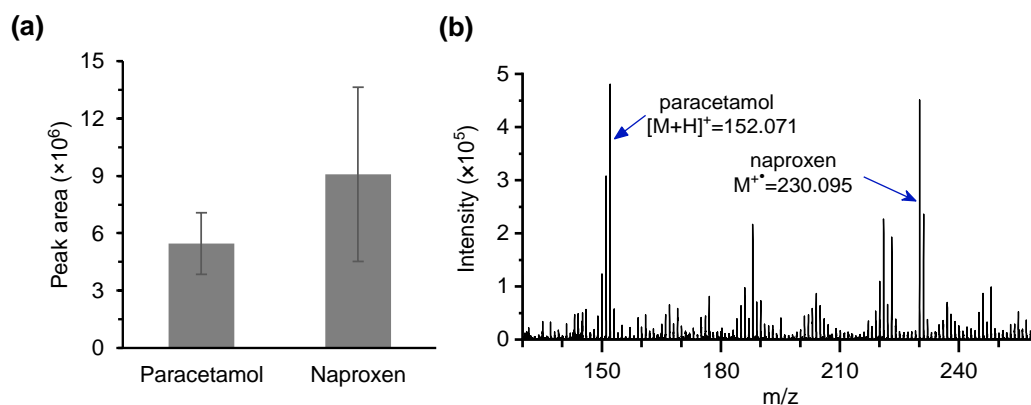


**Figure 23** (a) Comparison of the repeatability ( $n = 3$  LLE experiments) of intensities of extracted paracetamol (initial amount 300 pmol) and naproxen (initial amount 200 pmol) after LLE and evaporation of the final aqueous acceptor solution. (b) Mass spectra of the final acceptor solution featuring abundant paracetamol and naproxen ions. Modified and reprinted from ref. [117], © 2018 by Sathyanarayanan et al.; MDPI, CC BY 4.0.

## 5.4 Digital microfluidics for determining personalized drug clearance

The portability, scalability, and versatility of DMF technology has enabled it to be used for the rapid on-field diagnosis of infectious diseases<sup>[16]</sup> and newly born screenings for congenital diseases.<sup>[136]</sup> The key characteristics of DMF that enables these diagnostic assays are: (i) very low consumption of reagents and solvents and thus, reduced cost of chemicals, (ii) automation of entire assay protocol, which significantly reduces human labor and interventions, (iii) portable and scalable as disposable cartridges via mass manufacturing process, such as metal printing and roll coating, and (iv) compatibility towards a wide variety of biological samples, such as plasma, serum, biopsy tissue, etc.<sup>[137]</sup> Therefore, DMF could be a potential new technology for personalized drug dosing on the basis of the patient's drug clearance capacity since the amount of donor enzymes needed to carry out CYP assays are limited, i.e., from liver-biopsies. Genetic CYP diagnostic tests can only be used to assess the genotype, but they do not reveal the true expression level or activity of the isoenzymes. Therefore, in this study, we examined the feasibility of DMF for measuring the true activities (impacted by both genetic and external factors) by screening individual and pooled donor liver samples using both DMF-based and conventional (microtube) enzyme incubation protocols. For this purpose, EROD was selected as the model reaction to assess the CYP1A activity of five individual donor HLMs (donor A–E) and compared with that of the artificial population average (pool of 20 donors). The on-chip assay design consists of four reaction droplets per donor HLM sample in parallel, as illustrated in Figure 24a and b.

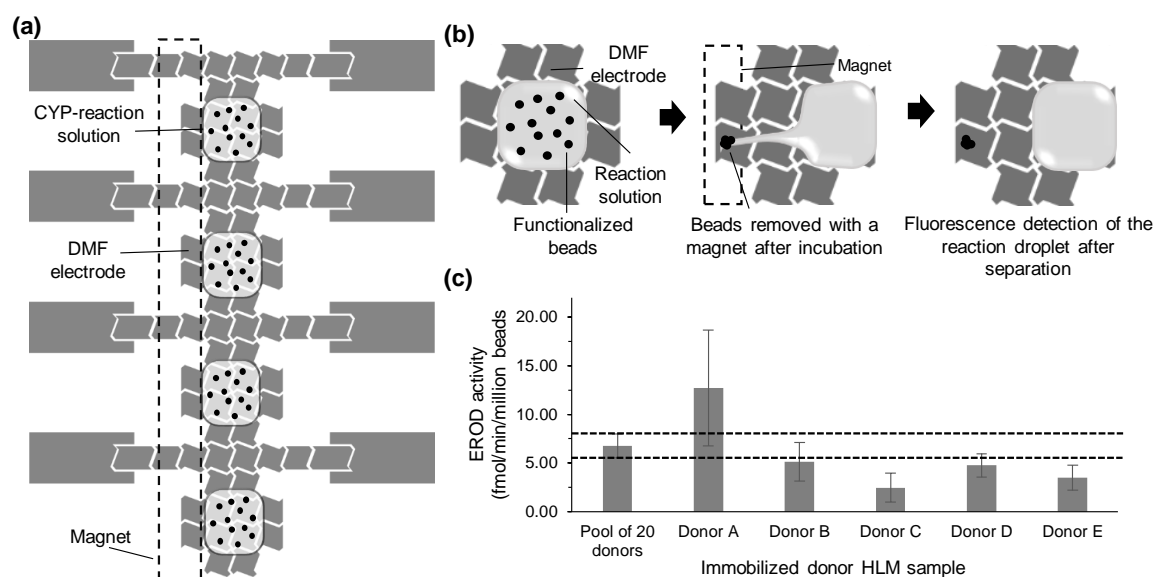


**Figure 24** (a) Schematic illustration of the bead-based DMF assay with four parallel reaction solutions for the CYP activity screening of donor HLMs. (b) Illustration of the separation protocol of beads from a single reaction droplet on the DMF device. (c) EROD activity of immobilized HLMs of individual donors (Donor A–E) and artificial pool of 20 donors; error bars: SD from  $n = 4$  assays.

Each reaction droplet was locally heated with a microheater featuring a multi-heater pattern, thanks to the region-specific heating of inkjet-printed microheaters (Figure 9b). Figure 24c shows the substantial variation in CYP1A activity of donor samples, among which activity of donors C and E are statistically significant ( $p = 0.004$  and  $0.009$ , respectively) than that of the average population (artificial pool of 20 donors). The detailed method validation data can be found in Publication IV. This suggests that the developed method is feasible to detect the variation in CYP activities of different individuals at droplet-scale with reduced enzyme and reagent consumption. In this method, only  $15\ \mu\text{g}$  of HLM protein per assay is needed (amount needed for the immobilization protocol, not the actual amount of immobilized proteins on beads) to functionalize  $\sim 1$  million beads, the amount used in one assay. Thus, the developed DMF-based CYP screening could be performed with a small fraction of liver biopsy from patients who undergo biopsy procedure due to critical illness.

## 6 Summary and conclusions

In this thesis, the possibility of carrying out drug metabolism research in droplet-scale using DMF technology was studied. This was demonstrated with drug metabolism assays, including on-chip metabolite identification as part of pre-clinical drug development and the CYP-activity screening of patient samples as part of post-clinical safety treatment (precision medicine).

In Publication I, droplet-scale CYP-IMERS were developed on a DMF platform for the on-chip metabolic profiling of drugs. Critical aspects related to CYP assays in droplet-scale were addressed: (i) incubation at physiological temperature was carried out using an integrated inkjet-printed microheater and (ii) low yield of CYP reactions were addressed by implementing porous polymer monoliths to increase the surface area for CYP-immobilization. The inkjet-printed microheater allowed localized heating of the CYP reactors on DMF device and allowed for the customization of assay designs on demand. Interfacing with a wellplate reader was straightforward and allowed for the fluorescence detection of metabolites without special microscope-PMT systems, which are common in microchannel-based devices.

Mass spectrometry is the gold standard for the non-targeted analysis of molecules and it is extensively used in metabolite identification during the drug discovery process. In Publication II, the DMF-based CYP reactor was integrated with ambient MS via DAPPI. The samples were directly analyzed from the DMF device without any need to integrate additional components, such as ESI emitters or capillaries for ionization. The interfacing of DMF with DAPPI-MS was possible by using highly stable SU-8 as the dielectric layer, which tolerated the high temperature vapor-jet during the desorption/ionization process. Also, drying the sample on SU-8 hydrophilic spots played a crucial role in the uniformity of sample precipitation, which in turn improved the repeatability of the desorption/ionization process. The developed method was sensitive enough to detect few pmol of drug metabolites produced from on-chip metabolism assays, as well as the drugs extracted from the on-chip distribution assays. DAPPI-MS is inherently a qualitative method and therefore, the developed DMF-DAPPI-MS method is not feasible for the quantitation of metabolites. Alternatively, this method can be used in the early stages of drug development by determining the solubility of drugs via LLE and identification of the most abundant metabolites of several isoenzymes via parallel reactions.

The DMF based sample preparation or assays need interfacing with a microchannel if the separation of analytes is required prior to analysis. However, integrating channel microfluidics with DMF is not straightforward and requires time-consuming and expensive cleanroom manufacturing processes, such as glass micromachining and bonding. In Publication III, a digital-to-channel microfluidic interface was achieved by using thiol-ene as a novel dielectric material for DMF. Thiol-ene was used both as a dielectric layer and the microchannel layer, which facilitated a straightforward thiol-ene-on-thiol-ene bonding. Thiol-enes, being solvent-free, enabled a much smoother surface upon coating on the porous Novele substrate used for inkjet-printing. Moreover, inkjet-printed electrodes served both as DMF actuation electrodes and MCE electrodes exposed on thiol-ene dielectric layer, thanks to the UV-patternability of thiol-enes. This interface was developed with careful

consideration into the fabrication processes, such as spin-coating, UV-curing and patterning, microchannel replication and bonding, which are processes that could potentially be transferable to high volume mass-manufacturing. Although the developed interface was not applied to drug metabolism studies in the context of this thesis yet, the preliminary characterization with fluorescent standards evidenced robust performance of the developed digital-to-channel microdevice with a view to rapid online analysis of DMF reactions.

In Publication IV, the DMF-based CYP assays were used to assess the patient-to-patient variation in CYP metabolic capacity. Four parallel assays were carried out and the region-specific heating of each reaction droplets was made possible with a microheater design featuring multiple-meandering patterns. Patient derived HLM samples were immobilized on magnetic beads and the functionalized beads were retrieved after the assays, which makes the DMF device reusable, unlike fixed monolith-based devices. In this case, thiol-ene was selected as dielectric material, which allowed the optical detection of metabolites also in the UV range, at which SU-8 gives substantial fluorescence background due to auto-fluorescence. The amount of sample needed was 15  $\mu\text{g}$  of total protein per assay, suggesting that this method is feasible for assessing the CYP activity using biopsy samples. The developed method was sensitive enough to determine the variation in individuals' CYP activities. With the automation and portability of DMF technology, this method could potentially be adapted in near-clinical laboratories with a view towards precision medicine for the screening of CYP activities for critically-ill patients.

In conclusion, the novel contributions arising from this work included several improvements in the cleanroom-free microfabrication and interfacing of DMF devices, and introducing DMF to a completely new application field focusing on the drug metabolism in human. Although high-throughput requirements were specifically not addressed in this study, the developed DMF-based systems are the initial steps towards the conceptualization of droplet-scale drug metabolism research. This thesis addressed the technological challenges in bringing down the drug metabolism research to droplet-scale by: (i) selecting DMF dielectric materials that are compatible with different detection methods to analyze lower amounts of metabolites, (ii) immobilization of enzymes (membrane proteins) on solid supports to increase the yield of the reactions on DMF, (iii) integrating on-demand microheaters for the localized heating of enzymatic reaction, and (iv) fabricating and interfacing devices with cleanroom-free, inexpensive, bench-top techniques to make them adaptable in common laboratory conditions. The developed droplet-scale systems can potentially contribute to pre-clinical drug development by significantly reducing the time, cost, and usage/wastage of expensive chemicals. In addition, the droplet-scale CYP activity screening can potentially be implemented as a diagnostic tool for the precision dosing of life-saving medicines. The DMF-based methods developed in this thesis in their present form are qualitative or semi-quantitative and therefore, could not readily be used for the prediction of kinetic parameters, such as intrinsic clearance ( $CL_{\text{int}}$ ) or  $IC_{50}$  inhibition constant. For that to be achieved, more focus in the future is needed on improving quantification limits, as well as the repeatability of the immobilization process w.r.t. the amount of immobilized enzymes per unit surface area. Also, the throughput of the current systems should be addressed to be on par with that of the state-of-the-art wellplate technologies that are routinely used in modern drug discovery.

## References

- [1] S. T. Susa, C. V. Preuss, in *StatPearls*, StatPearls Publishing, Treasure Island (FL), **2020**.
- [2] S. Ou-Yang, J. Lu, X. Kong, Z. Liang, C. Luo, H. Jiang, *Acta Pharmacologica Sinica* **2012**, 33, 1131.
- [3] J. Kirchmair, A. H. Göller, D. Lang, J. Kunze, B. Testa, I. D. Wilson, R. C. Glen, G. Schneider, *Nature Reviews Drug Discovery* **2015**, 14, 387.
- [4] D. S. Wishart, *Nature Reviews Drug Discovery* **2016**, 15, 473.
- [5] U. M. Zanger, M. Schwab, *Pharmacology & Therapeutics* **2013**, 138, 103.
- [6] F. P. Guengerich, *Chem. Res. Toxicol.* **2008**, 21, 70.
- [7] H. Matthews, J. Hanison, N. Nirmalan, *Proteomes* **2016**, 4, 28.
- [8] D. R. Reyes, D. Iossifidis, P.-A. Auroux, A. Manz, *Anal. Chem.* **2002**, 74, 2623.
- [9] S. J. Lee, S. Y. Lee, *Appl Microbiol Biotechnol* **2004**, 64, 289.
- [10] R. Daw, J. Finkelstein, *Nature* **2006**, 442, 367.
- [11] P. S. Dittrich, A. Manz, *Nature Reviews Drug Discovery* **2006**, 5, 210.
- [12] K. Choi, A. H. C. Ng, R. Fobel, A. R. Wheeler, *Annual Review of Analytical Chemistry* **2012**, 5, 413.
- [13] Z.-G. Guo, F. Zhou, J.-C. Hao, Y.-M. Liang, W.-M. Liu, W. T. S. Huck, *Appl. Phys. Lett.* **2006**, 89, 081911.
- [14] Z. Guttenberg, H. Müller, H. Habermüller, A. Geisbauer, J. Pipper, J. Felbel, M. Kielpinski, J. Scriba, A. Wixforth, *Lab Chip* **2005**, 5, 308.
- [15] A. A. Darhuber, J. P. Valentino, S. M. Troian, S. Wagner, *Journal of Microelectromechanical Systems* **2003**, 12, 873.
- [16] A. H. C. Ng, R. Fobel, C. Fobel, J. Lamanna, D. G. Rackus, A. Summers, C. Dixon, M. D. M. Dryden, C. Lam, M. Ho, N. S. Mufti, V. Lee, M. A. M. Asri, E. A. Sykes, M. D. Chamberlain, R. Joseph, M. Ope, H. M. Scobie, A. Knipes, P. A. Rota, N. Marano, P. M. Chege, M. Njuguna, R. Nzunza, N. Kisangau, J. Kiogora, M. Karuingi, J. W. Burton, P. Borus, E. Lam, A. R. Wheeler, *Science Translational Medicine* **2018**, 10, eaar6076.
- [17] M. J. Jebrail, A. R. Wheeler, *Current Opinion in Chemical Biology* **2010**, 14, 574.
- [18] G. M. Whitesides, *Nature* **2006**, 442, 368.
- [19] S.-Y. Teh, R. Lin, L.-H. Hung, A. P. Lee, *Lab on a Chip* **2008**, 8, 198.
- [20] M. Washizu, *IEEE Transactions on Industry Applications* **1998**, 34, 732.
- [21] M. G. Pollack, A. D. Shenderov, R. B. Fair, *Lab on a Chip* **2002**, 2, 96.
- [22] M. G. Pollack, R. B. Fair, A. D. Shenderov, *Appl. Phys. Lett.* **2000**, 77, 1725.
- [23] S. K. Cho, H. Moon, C.-J. Kim, *Journal of Microelectromechanical Systems* **2003**, 12, 70.
- [24] E. Orabona, A. Calìò, I. Rendina, L. D. Stefano, M. Medugno, *Micromachines* **2013**, 4, 206.
- [25] D.-K. Kang, M. Monsur Ali, K. Zhang, E. J. Pone, W. Zhao, *TrAC Trends in Analytical Chemistry* **2014**, 58, 145.
- [26] M. E. Razu, J. Kim, in *2017 IEEE 30th International Conference on Micro Electro Mechanical Systems (MEMS)*, **2017**, pp. 1333–1336.
- [27] H. Ko, J. Lee, Y. Kim, B. Lee, C.-H. Jung, J.-H. Choi, O.-S. Kwon, K. Shin, *Advanced Materials* **2014**, 26, 2335.
- [28] M. W. L. Watson, M. Abdelgawad, G. Ye, N. Yonson, J. Trottier, A. R. Wheeler, *Anal. Chem.* **2006**, 78, 7877.
- [29] J. Gong, C.-J. Kim, *Journal of Microelectromechanical Systems* **2008**, 17, 257.
- [30] R. Fobel, A. E. Kirby, A. H. C. Ng, R. R. Farnood, A. R. Wheeler, *Advanced Materials* **2014**, 26, 2838.
- [31] H. Liu, S. Dharmatilleke, D. K. Maurya, A. A. O. Tay, *Microsyst Technol* **2009**, 16, 449.
- [32] J.-H. Wei, W.-S. Hsu, S.-K. Fan, in *2007 2nd IEEE International Conference on Nano/Micro Engineered and Molecular Systems*, **2007**, pp. 981–984.
- [33] D. Brassard, L. Malic, F. Normandin, M. Tabrizian, T. Veres, *Lab on a Chip* **2008**, 8, 1342.
- [34] M. Abdelgawad, A. R. Wheeler, *Advanced Materials* **2007**, 19, 133.
- [35] C. Dixon, A. H. C. Ng, R. Fobel, M. B. Miltenburg, A. R. Wheeler, *Lab on a Chip* **2016**, 16, 4560.
- [36] R. Fobel, C. Fobel, A. R. Wheeler, *Appl. Phys. Lett.* **2013**, 102, 193513.
- [37] M. Alistar, U. Gaudenz, *Bioengineering* **2017**, 4, 45.
- [38] E. M. Miller, A. H. C. Ng, U. Uddayasankar, A. R. Wheeler, *Anal Bioanal Chem* **2011**, 399, 337.
- [39] S. H. Au, S. C. C. Shih, A. R. Wheeler, *Biomed Microdevices* **2011**, 13, 41.

- [40] R. S. Sista, A. E. Eckhardt, V. Srinivasan, M. G. Pollack, S. Palanki, V. K. Pamula, *Lab Chip* **2008**, 8, 2188.
- [41] M. D. M. Dryden, D. D. G. Rackus, M. H. Shamsi, A. R. Wheeler, *Anal. Chem.* **2013**, 85, 8809.
- [42] M. H. Shamsi, K. Choi, A. H. C. Ng, A. R. Wheeler, *Lab on a Chip* **2014**, 14, 547.
- [43] S. C. C. Shih, I. Barbulovic-Nad, X. Yang, R. Fobel, A. R. Wheeler, *Biosensors and Bioelectronics* **2013**, 42, 314.
- [44] A. E. Kirby, A. R. Wheeler, *Anal. Chem.* **2013**, 85, 6178.
- [45] A. R. Wheeler, H. Moon, C. A. Bird, R. R. Ogorzalek Loo, C.-J. “C. J.” Kim, J. A. Loo, R. L. Garrell, *Anal. Chem.* **2005**, 77, 534.
- [46] J. Heinemann, K. Deng, S. C. C. Shih, J. Gao, P. D. Adams, A. K. Singh, T. R. Northen, *Lab Chip* **2017**, 17, 323.
- [47] S. C. C. Shih, H. Yang, M. J. Jebrail, R. Fobel, N. McIntosh, O. Y. Al-Dirbashi, P. Chakraborty, A. R. Wheeler, *Anal. Chem.* **2012**, 84, 3731.
- [48] M. Abdelgawad, M. W. L. Watson, A. R. Wheeler, *Lab on a Chip* **2009**, 9, 1046.
- [49] M. W. L. Watson, M. J. Jebrail, A. R. Wheeler, *Anal. Chem.* **2010**, 82, 6680.
- [50] S. C. C. Shih, P. C. Gach, J. Sustarich, B. A. Simmons, P. D. Adams, S. Singh, A. K. Singh, *Lab Chip* **2014**, 15, 225.
- [51] F. Ahmadi, K. Samlali, P. Q. N. Vo, S. C. C. Shih, *Lab Chip* **2019**, 19, 524.
- [52] L. Malic, T. Veres, M. Tabrizian, *Biosensors and Bioelectronics* **2009**, 24, 2218.
- [53] K.-M. Lei, P.-I. Mak, M.-K. Law, R. P. Martins, *Analyst* **2014**, 139, 6204.
- [54] H. Ding, S. Sadeghi, G. J. Shah, S. Chen, P. Y. Keng, C.-J. “CJ” Kim, R. M. van Dam, *Lab Chip* **2012**, 12, 3331.
- [55] M. J. Jebrail, A. H. C. Ng, V. Rai, R. Hili, A. K. Yudin, A. R. Wheeler, *Angewandte Chemie International Edition* **2010**, 49, 8625.
- [56] K. P. Nichols, J. G. E. Gardeniers, *Anal. Chem.* **2007**, 79, 8699.
- [57] J. G. Martin, M. Gupta, Y. Xu, S. Akella, J. Liu, J. S. Dordick, R. J. Linhardt, *J. Am. Chem. Soc.* **2009**, 131, 11041.
- [58] A. H. C. Ng, M. Lee, K. Choi, A. T. Fischer, J. M. Robinson, A. R. Wheeler, *Clin Chem* **2015**, 61, 420.
- [59] M. J. Jebrail, A. R. Wheeler, *Anal. Chem.* **2009**, 81, 330.
- [60] D. Chatterjee, A. J. Ytterberg, S. U. Son, J. A. Loo, R. L. Garrell, *Anal. Chem.* **2010**, 82, 2095.
- [61] J. Kim, S. Abdulwahab, K. Choi, N. M. Lafrenière, J. M. Mudrik, H. Gomaa, H. Ahmado, L.-A. Behan, R. F. Casper, A. R. Wheeler, *Anal. Chem.* **2015**, 87, 4688.
- [62] S. Abdulwahab, A. H. C. Ng, M. D. Chamberlain, H. Ahmado, L.-A. Behan, H. Gomaa, R. F. Casper, A. R. Wheeler, *Lab Chip* **2017**, 17, 1594.
- [63] Y.-J. Liu, D.-J. Yao, H.-C. Lin, W.-Y. Chang, H.-Y. Chang, *J. Micromech. Microeng.* **2008**, 18, 045017.
- [64] Y.-H. Chang, G.-B. Lee, F.-C. Huang, Y.-Y. Chen, J.-L. Lin, *Biomed Microdevices* **2006**, 8, 215.
- [65] S. Kalsi, M. Valiadi, M.-N. Tsaloglou, L. Parry-Jones, A. Jacobs, R. Watson, C. Turner, R. Amos, B. Hadwen, J. Buse, C. Brown, M. Sutton, H. Morgan, *Lab Chip* **2015**, 15, 3065.
- [66] I. Barbulovic-Nad, H. Yang, P. S. Park, A. R. Wheeler, *Lab Chip* **2008**, 8, 519.
- [67] A. H. C. Ng, M. D. Chamberlain, H. Situ, V. Lee, A. R. Wheeler, *Nature Communications* **2015**, 6, 1.
- [68] A. P. Aijian, R. L. Garrell, *J Lab Autom* **2015**, 20, 283.
- [69] S. L. S. Freire, *Sensors and Actuators A: Physical* **2016**, 250, 15.
- [70] W. van der Vegt, W. Norde, H. C. van der Mei, H. J. Busscher, *Journal of Colloid and Interface Science* **1996**, 179, 57.
- [71] V. N. Luk, G. CH. Mo, A. R. Wheeler, *Langmuir* **2008**, 24, 6382.
- [72] A. Christiansen, T. Backensfeld, K. Denner, W. Weitschies, *European Journal of Pharmaceutics and Biopharmaceutics* **2011**, 78, 166.
- [73] E. Ollikainen, D. Liu, A. Kallio, E. Mäkilä, H. Zhang, J. Salonen, H. A. Santos, T. M. Sikanen, *European Journal of Pharmaceutical Sciences* **2017**, 104, 124.
- [74] P. Q. N. Vo, M. C. Husser, F. Ahmadi, H. Sinha, S. C. C. Shih, *Lab on a Chip* **2017**, 17, 3437.
- [75] M. J. Jebrail, R. F. Renzi, A. Sinha, J. V. D. Vreugde, C. Gondhalekar, C. Ambriz, R. J. Meagher, S. S. Branda, *Lab Chip* **2014**, 15, 151.

- [76] Fei Su, W. Hwang, K. Chakrabarty, in *Proceedings of the Design Automation Test in Europe Conference*, **2006**, pp. 1–6.
- [77] M. J. Jebrail, N. Assem, J. M. Mudrik, M. D. M. Dryden, K. Lin, A. K. Yudin, A. R. Wheeler, *J Flow Chem* **2012**, 2, 103.
- [78] S. H. Au, M. Dean Chamberlain, S. Mahesh, M. V. Sefton, A. R. Wheeler, *Lab on a Chip* **2014**, 14, 3290.
- [79] E. Moazami, J. M. Perry, G. Soffer, M. C. Husser, S. C. C. Shih, *Anal. Chem.* **2019**, 91, 5159.
- [80] S. C. C. Shih, G. Goyal, P. W. Kim, N. Koutsoubelis, J. D. Keasling, P. D. Adams, N. J. Hillson, A. K. Singh, *ACS Synth. Biol.* **2015**, 4, 1151.
- [81] S. Srigunapalan, I. A. Eydelnant, C. A. Simmons, A. R. Wheeler, *Lab Chip* **2011**, 12, 369.
- [82] “Human Cytochrome P450s,” can be found under <http://drnelson.uthsc.edu/human.P450.table.html>, accessed on Mar **2020**.
- [83] U. M. Zanger, M. Turpeinen, K. Klein, M. Schwab, *Anal Bioanal Chem* **2008**, 392, 1093.
- [84] D. W. Nebert, D. W. Russell, *The Lancet* **2002**, 360, 1155.
- [85] J. Bajorath, *Nat Rev Drug Discov* **2002**, 1, 882.
- [86] M. Ruokolainen, T. Gul, H. Permentier, T. Sikanen, R. Kostainen, T. Kotiaho, *European Journal of Pharmaceutical Sciences* **2016**, 83, 36.
- [87] R. A. Stringer, C. Strain-Damerell, P. Nicklin, J. B. Houston, *Drug Metabolism & Disposition* **2009**, 37, 1025.
- [88] S. Asha, M. Vidyavathi, *Appl Biochem Biotechnol* **2010**, 160, 1699.
- [89] G. Tuschl, B. Lauer, S. O. Mueller, *Expert Opinion on Drug Metabolism & Toxicology* **2008**, 4, 855.
- [90] A. Costa, B. Sarmento, V. Seabra, *Expert Opinion on Drug Metabolism & Toxicology* **2014**, 10, 103.
- [91] J. Moaddeb, S. B. Haga, *Ther Adv Drug Saf* **2013**, 4, 155.
- [92] V. P. Androutsopoulos, A. M. Tsatsakis, D. A. Spandidos, *BMC Cancer* **2009**, 9, 187.
- [93] A. Anwar-Mohamed, R. H. Elbekai, A. O. El-Kadi, *Expert Opin Drug Metab Toxicol* **2009**, 5, 501.
- [94] K. Abass, O. Pelkonen, *Toxicol In Vitro* **2013**, 27, 1584.
- [95] M. Hamilton, J. L. Wolf, J. Rusk, S. E. Beard, G. M. Clark, K. Witt, P. J. Cagnoni, *Clin Cancer Res* **2006**, 12, 2166.
- [96] P. Cui, S. Wang, *J Pharm Anal* **2019**, 9, 238.
- [97] S. Damiani, U. B. Kompella, S. A. Damiani, R. Kodzius, *Genes* **2018**, 9, 103.
- [98] J. R. Kraly, R. E. Holcomb, Q. Guan, C. S. Henry, *Analytica Chimica Acta* **2009**, 653, 23.
- [99] J. B. Lee, J. H. Sung, *Biotechnology Journal* **2013**, 8, 1258.
- [100] R. Nicolini, M. Bartolini, S. Rudaz, V. Andrisano, J.-L. Veuthey, *Journal of Chromatography A* **2008**, 1206, 2.
- [101] C. Y. Chan, P.-H. Huang, F. Guo, X. Ding, V. Kapur, J. D. Mai, P. K. Yuen, T. J. Huang, *Lab Chip* **2013**, 13, 4697.
- [102] S. Matosevic, N. Szita, F. Baganz, *J. Chem. Technol. Biotechnol.* **2011**, 86, 325.
- [103] J. Schejbal, R. Řemínek, L. Zeman, A. Mádr, Z. Glatz, *Journal of Chromatography A* **2016**, 1437, 234.
- [104] S. M. Sukumaran, B. Potsaid, M. Lee, D. S. Clark, J. S. Dordick, *J Biomol Screen* **2009**, 14, 668.
- [105] C. Mateo, J. M. Palomo, G. Fernandez-Lorente, J. M. Guisan, R. Fernandez-Lafuente, *Enzyme and Microbial Technology* **2007**, 40, 1451.
- [106] E. Jutila, R. Koivunen, I. Kiiski, R. Bollström, T. Sikanen, P. Gane, *Advanced Functional Materials* **2018**, 28, 1802793.
- [107] E. W. Esch, A. Bahinski, D. Huh, *Nature Reviews Drug Discovery* **2015**, 14, 248.
- [108] I. Kiiski, T. Pihlaja, L. Urvas, S. Wiedmer, V. Jokinen, T. Sikanen, *Advanced Biosystems* **2019**, 3, 1800245.
- [109] T. M. Sikanen, J. P. Lafleur, M.-E. Moilanen, G. Zhuang, T. G. Jensen, J. P. Kutter, *J. Micromech. Microeng.* **2013**, 23, 037002.
- [110] C. Fredrik Carlborg, T. Haraldsson, K. Öberg, M. Malkoch, W. van der Wijngaart, *Lab on a Chip* **2011**, 11, 3136.
- [111] I. Swyer, R. Fobel, A. R. Wheeler, *Langmuir* **2019**, 35, 5342.
- [112] J. Zhou, S. M. Poloyac, *Expert Opin Drug Metab Toxicol* **2011**, 7, 803.
- [113] T. Sikanen, T. Zwinger, S. Tuomikoski, S. Franssila, R. Lehtiniemi, C.-M. Fager, T. Kotiaho, A. Pursula, *Microfluid Nanofluid* **2008**, 5, 479.
- [114] G. Sathyanarayanan, M. Haapala, I. Kiiski, T. Sikanen, *Anal Bioanal Chem* **2018**, 410, 6677.

- [115] J. P. Lafleur, S. Senkbeil, J. Novotny, G. Nys, N. Bøgelund, K. D. Rand, F. Foret, J. P. Kutter, *Lab Chip* **2015**, *15*, 2162.
- [116] A. H. C. Ng, K. Choi, R. P. Luoma, J. M. Robinson, A. R. Wheeler, *Anal. Chem.* **2012**, *84*, 8805.
- [117] G. Sathyanarayanan, M. Haapala, T. Sikanen, *Micromachines* **2018**, *9*, 649.
- [118] G. Sathyanarayanan, P. Järvinen, T. Sikanen, “APPLICATION NOTE: Quantification of digital microfluidic fluorescence assays with the Varioskan LUX Multimode Microplate Reader,” can be found under <http://assets.thermofisher.com/TFS-Assets/BID/Application-Notes/digital-microfluidics-chips-varioskan-LUX-app-note.PDF>, **2018**.
- [119] M. Haapala, J. Pöl, V. Saarela, V. Arvola, T. Kotiaho, R. A. Ketola, S. Franssila, T. J. Kauppila, R. Kostiainen, *Anal. Chem.* **2007**, *79*, 7867.
- [120] V. Saarela, M. Haapala, R. Kostiainen, T. Kotiaho, S. Franssila, *Lab Chip* **2007**, *7*, 644.
- [121] G. Sathyanarayanan, M. Haapala, C. Dixon, A. R. Wheeler, T. M. Sikanen, *Advanced Materials Technologies* **2020**, 2000451.
- [122] K. L. Choy, *Progress in Materials Science* **2003**, *48*, 57.
- [123] J. Xu, C. P. Wong, *Journal of Applied Polymer Science* **2007**, *103*, 1523.
- [124] J. Min Ko, Y. Hun Kang, C. Lee, S. Yun Cho, *Journal of Materials Chemistry C* **2013**, *1*, 3091.
- [125] O. D. McNair, A. P. Janisse, D. E. Krzeminski, D. E. Brent, T. E. Gould, J. W. Rawlins, D. A. Savin, *ACS Appl. Mater. Interfaces* **2013**, *5*, 11004.
- [126] R. Feng, R. J. Farris, *J. Micromech. Microeng.* **2002**, *13*, 80.
- [127] Y.-F. Li, Y.-J. Sheng, H.-K. Tsao, *Langmuir* **2013**, *29*, 7802.
- [128] S. Tuomikoski, S. Franssila, *Sensors and Actuators A: Physical* **2005**, *120*, 408.
- [129] S. Senkbeil, J. Aho, L. Yde, L. R. Lindvold, J. F. Stensborg, J. Rantanen, J. P. Lafleur, J. P. Kutter, *J. Micromech. Microeng.* **2016**, *26*, 075014.
- [130] A. Mohammadi-Bardbori, *Protocol Exchange* **2014**.
- [131] T. Chen, Y. Jia, C. Dong, J. Gao, P.-I. Mak, R. P. Martins, *Lab on a Chip* **2016**, *16*, 743.
- [132] W.-K. Huang, H.-L. Chen, S.-K. Fan, in *19th International Conference on Miniaturized Systems for Chemistry and Life Sciences*, **2015**, pp. 85–87.
- [133] Y. Fouillet, D. Jary, C. Chabrol, P. Claustre, C. Peponnet, *Microfluid Nanofluid* **2008**, *4*, 159.
- [134] L. Luosujärvi, V. Arvola, M. Haapala, Jaroslav Pöl, V. Saarela, S. Franssila, T. Kotiaho, R. Kostiainen, T. J. Kauppila, *Anal. Chem.* **2008**, *80*, 7460.
- [135] P. A. L. Wijethunga, Y. S. Nanayakkara, P. Kunchala, D. W. Armstrong, H. Moon, *Anal. Chem.* **2011**, *83*, 1658.
- [136] D. Millington, S. Norton, R. Singh, R. Sista, V. Srinivasan, V. Pamula, *Expert Rev Mol Diagn* **2018**, *18*, 701.
- [137] D. S. Millington, R. Sista, A. Eckhardt, J. Rouse, D. Bali, R. Goldberg, M. Cotten, R. Buckley, V. Pamula, *Seminars in Perinatology* **2010**, *34*, 163.





**ISBN 978-951-51-6453-7 (PRINT)**  
**ISBN 978-951-51-6454-4 (ONLINE)**  
**ISSN 2669-882X (PRINT)**  
**ISSN 2670-2010 (ONLINE)**  
**<http://ethesis.helsinki.fi>**

**HELSINKI 2020**